Differential contribution of two organelles of endosymbiotic origin to iron-sulfur cluster synthesis in Toxoplasma

Sarah Pamukcu[1], Aude Cerutti[1], Sonia Hem[2], Valérie Rofidal[2], Sébastien Besteiro[3*]

[1]LPHI, Univ Montpellier, CNRS, Montpellier, France

[2]BPMP, Univ Montpellier, CNRS, INRAE, Institut Agro, Montpellier, France

[3]LPHI, Univ Montpellier, CNRS, INSERM, Montpellier, France

* sebastien.besteiro@inserm.fr

Abstract

Iron-sulfur (Fe-S) clusters are one of the most ancient and ubiquitous prosthetic groups, and they are required by a variety of proteins involved in important metabolic processes. Apicomplexan parasites have inherited different plastidic and mitochondrial Fe-S clusters biosynthesis pathways through endosymbiosis. We have investigated the relative contributions of these pathways to the fitness of *Toxoplasma gondii*, an apicomplexan parasite causing disease in humans, by generating specific mutants. Phenotypic analysis and quantitative proteomics allowed us to highlight striking differences in these mutants. Both Fe-S cluster synthesis pathways are necessary for optimal parasite growth in vitro, but their disruption leads to markedly different fates: impairment of the plastidic pathway leads to a loss of the organelle and to parasite death, while disruption of the mitochondrial pathway trigger differentiation into a stress resistance stage. This highlights that otherwise similar biochemical pathways hosted by different sub-cellular compartments can have very different contributions to the biology of the parasites, which is something to consider when exploring novel strategies for therapeutic intervention.

Keywords: iron sulfur cluster, Toxoplasma, differentiation, bradyzoite, apicoplast, mitochondrion

Introduction

Endosymbiotic events were crucial in the evolutionary timeline of eukaryotic cells. Mitochondria and plastids evolved from free-living prokaryotes that were taken up by early eukaryotic ancestors and transformed into permanent subcellular compartments that have become essential for harnessing energy or synthesizing essential metabolites in present-day eukaryotes (1). As semiautonomous organelles, they contain a small genome, but during the course of evolution a considerable part of their genes have been transferred to the cell nucleus. Yet, they rely largely on nuclear factors for their maintenance and expression. Both organelles are involved in critically important biochemical processes. Mitochondria, which are found in most eukaryotic organisms, are mostly known as the powerhouses of the cell, owing to their ability to produce ATP through respiration. Importantly, they are also involved in several other metabolic pathways (2), including the synthesis of heme groups, steroids, amino acids, and iron-sulphur (Fe-S) clusters. Moreover, they have important cellular functions in regulating redox and calcium homeostasis. Similarly, plastids that are found in plants, algae and some other eukaryotic organisms host a diverse array of pathways that contribute greatly

to the cellular metabolism (3). While often identified mainly as compartments where photosynthesis occurs, plastids host many more metabolic pathways. For example, they are involved in the assimilation of nitrogen and sulfur, as well as the synthesis of carbohydrates, amino acids, fatty acids and specific lipids, hormone precursors, and also Fe-S clusters. The best-characterized plastid is arguably the plant cell chloroplast, but not all plastids have photosynthetic function, and in higher plants they are in fact a diverse group of organelles that share basal metabolic pathways, but also have specific physiological roles (4). As documented in plants, although mitochondria and plastids are highly compartmentalized (5), they have metabolic exchanges and cooperate in the context of several important metabolic pathways (6).

The phylum Apicomplexa comprises a large number of single-celled protozoan parasites responsible for cause serious disease in animals and humans. For example, this phylum includes parasites of the genus *Plasmodium* that are responsible for the deadly malaria, and *Toxoplasma gondii* a ubiquitous parasite that can lead to a severe pathology in immunocompromised individuals. Apicomplexan parasites evolved from a photosynthetic ancestor and many of them still retain a plastid (7, 8). This plastid, named the apicoplast, originated from a secondary endosymbiotic event: the eukaryotic ancestor of Apicomplexa engulfed and retained a eukaryotic alga that was already containing a plastid obtained by primary endosymbiosis of a cyanobacterium-like prokaryote (9, 10). It has lost its photosynthetic properties as the ancestors of Apicomplexa switched to an intracellular parasitic lifestyle (11). The apicoplast nevertheless still hosts four main metabolic pathways (12, 13): a 2-C-methyl-D-erythritol 4-phosphate/1-deoxy-d-xylulose 5-phosphate (MEP/DOXP) pathway for the synthesis of isoprenoid precursors, a type II fatty acid synthesis pathway (FASII), part of the heme synthesis pathway, and a Fe-S cluster synthesis pathway. As the apicoplast is involved in these vital biological processes for the parasite, and as they markedly differ from those of the host (because of their algal origin), that makes it a valuable potential drug target. Apicomplexan parasites also generally contain a single tubular mitochondrion, although its aspect may vary during parasite development (14, 15). The organelle is an important contributor to the parasites metabolic needs (16). It classically hosts tricarboxylic acid (TCA) cycle reactions, which are the main source of electrons that feeds the mitochondrial electron transport chain (ETC) and generate a proton gradient used for ATP production. It also contains additional metabolic pathways, like a Fe-S cluster synthesis pathway and part of the heme synthesis pathway operating in collaboration with the apicoplast. The latter reflects obvious functional links between the organelles and potential metabolic interactions, which is also illustrated by their physical connection during parasite development (17, 18). Because of their endosymbiotic origin, these organelles offer possibilities for intervention against Apicomplexa and are currently the target of treatments (19). For instance, as their protein synthesis machinery is bacterial in nature, both may therefore be a target of bacterial translation inhibitors such as azithromycin, spiramycin or clindamycin (20). However, current evidence suggests that the apicoplast is the primary target of these drugs. The mitochondrion, on the other hand, is an important drug target through the ETC it harbours, which is inhibited by drugs such as atovaquone (21).

Fe-S clusters are simple and ubiquitous cofactors involved in a great variety of cellular processes. As their name implies, they are composed of iron and inorganic sulfur whose chemical properties confer key structural or electron transfer features to proteins in all kingdoms of life. They are important to the activities of numerous proteins that play essential roles to sustain fundamental life processes including, in addition to electron transfer and exchange, iron storage, protein folding, oxygen/nitrogen stress sensing, and gene regulation (22). The synthesis of Fe-S clusters and their insertion into apoproteins requires complex machineries and several distinct pathways have been

88 identified in bacteria for synthesizing these ancient cofactors (23). They include the ISC (iron sulfur
89 cluster) pathway for general Fe–S cluster assembly (24), and the SUF (sulfur formation) pathway (25)
90 that is potentially activated in oxidative stress conditions (26). Eukaryotes have inherited machineries
91 for synthesizing Fe-S cluster through their endosymbionts (27). As a result, organisms with both
92 mitochondria and plastids, like higher plants, use the ISC pathway for assembling Fe-S clusters in the
93 mitochondria and the SUF pathway for Fe-S clusters in the plastids (28). Additional protein
94 components that constitute a cytosolic Fe-S cluster assembly machinery (CIA) have also been
95 identified: this pathway is important for the generation of cytosolic, but also of nuclear Fe-S proteins,
96 and is highly dependent on the ISC mitochondrial pathway for providing a sulfur-containing precursor
97 (29).

98 Like in plants and algae, apicoplast-containing Apicomplexa seem to harbour the three ISC, SUF and
99 CIA Fe-S cluster synthesis pathways. Although the CIA pathway was recently shown to be important
100 for *Toxoplasma* fitness (30), investigations in apicomplexan parasites have been so far almost
101 exclusively focused on the apicoplast-located SUF pathway (31–35) and mostly in *Plasmodium*
102 species. The SUF pathway was shown to be essential for the viability of malaria parasites during both
103 the erythrocytic and sexual stages of development and has thus been recognized as a putative
104 avenue for discovering new antiparasitic drug targets (reviewed in (36)). Contrarily to the ISC
105 pathway, which is also present the mammalian hosts of apicomplexan parasites, the SUF pathway
106 may indeed yield interesting specificities that may be leveraged for therapeutic intervention.
107 However, very little is known about Fe-S clusters synthesis in other apicomplexan parasites, including
108 *T. gondii*. For instance, out of the four known metabolic pathways hosted by the apicoplast, Fe-S
109 synthesis was the only one remaining to be functionally investigated in *T. gondii*, while the others
110 were all shown to be essential for the tachyzoite stage of the parasite (a fast replicating
111 developmental stage responsible for the symptoms of the disease) (37–40). Here, we present the
112 characterization of two *T. gondii* mutants we generated to specifically impact the plastidic and
113 mitochondrial SUF and ISC pathways, respectively. Our goal was to assess the relative contributions
114 of these compartmentalized pathways to the parasite development and fitness.

115

116 **Results**

117 **TgSufS and TgIscU are functional homologs of components of the plastidic and mitochondrial iron**
118 **sulfur cluster synthesis pathways**

119 Fe-S cluster biosynthesis pathways in the mitochondrion and the plastid follow a similar general
120 pattern: cysteine desulfurases (IscS, SufS) produce sulfur from L-cysteine, scaffold proteins (IscU,
121 SufB/C/D) provide a molecular platform allowing iron and sulfur to meet and form a cluster, and
122 finally carrier proteins (like IscA or SufA) deliver the cluster to target apoproteins (28). The cytosolic
123 CIA pathway, which is responsible for the de novo formation of Fe-S clusters to be incorporated in
124 cytosolic and nuclear proteins, is dependent on the ISC pathway, as its first step requires the import
125 of a yet unknown sulfur-containing precursor that is translocated to the cytosol from the
126 mitochondrion (29). To get a general overview of the predicted components for the Fe-S cluster
127 machinery in *T. gondii*, we conducted homology searches in the ToxoDB.org database (41), using
128 well-characterized proteins from plants (*Arabidopsis thaliana*) belonging to the SUF, ISC and CIA
129 pathways (Table S1). Data from global mapping of protein subcellular location by HyperLOPIT spatial
130 proteomics (42) was in general in good accordance with the expected localization of the homologs
131 (with the noticeable exception of members of the NBP35/HCF101 ATP-binding proteins). Overall, our
132 search revealed that *T. gondii* appeared to have a good conservation of all the main components of

133 the three ISC, SUF and CIA Fe-S synthesis pathways (Table S1, Figure 1A). Additional information
134 available on ToxoDB.org such as scores from a CRISPR/Cas9-based genome-wide screening (43),
135 highlighted that most components of the three pathways are important for parasite fitness. This
136 suggests several apoproteins localizing to the endosymbiotic organelles, but also the cytosol/nucleus,
137 are essential for the optimal growth of tachyzoites.

138 In order to verify this, we decided to generate mutants of the apicoplast-localized SUF pathway and
139 of the mitochondrion-localized ISC pathway in *T. gondii* tachyzoites. To this end, we targeted the SufS
140 and IscU homologs, which are both central (and presumably essential) to their respective pathways
141 (Figure 1A). We first sought to verify TgSufS (TGGT1_216170) and TgIscU (TGGT1_237560) were real
142 functional homologs by performing complementation assays of bacterial mutants. Expression of the
143 predicted functional domains of TgSufS and TgIscU in the respective *Escherichia coli* mutants
144 improved bacterial growth in the presence of an iron chelator or not (Figure 1B). This suggests TgSufS
145 and TgIscU, in addition to a good sequence homology with their bacterial homologues (Figure S1),
146 have a conserved function.

147 We next determined the sub-cellular localizations of TgSufS and TgIscU by epitope tagging of the
148 native proteins. This was achieved in the TATi ΔKu80 cell line, which favors homologous
149 recombination and would allow transactivation of a Tet operator-modified promoter we would later
150 use for generating a conditional mutant in this background (44–46). A sequence coding for a C-
151 terminal triple hemagglutinin (HA) epitope tag was inserted at the endogenous *TgSufS* or *TgIscU*
152 locus by homologous recombination (Figure S2). Using the anti-HA antibody, by immunoblot we
153 detected two products for each protein (Figure 2A, B), likely corresponding to their immature and
154 mature forms (ie after cleavage of the transit peptide upon import into the organelle). Accordingly,
155 the analysis of TgSufS and TgIscU sequences with several subcellular localization and N-terminal
156 sorting signals site predictors confirmed they likely contained sequences for plastidic and
157 mitochondrial targeting (47), respectively, although no consensus position of the exact cleavage sites
158 could be determined. Immunofluorescence assay (IFA) in *T. gondii* tachyzoites confirmed HA-tagged
159 TgSufS and TgIscU co-localized with markers of the apicoplast and the mitochondrion, respectively
160 (Figure 2C, D).

161 SufS is a cysteine desulfurase whose activity is enhanced by an interaction with the SufE protein (48).
162 Similarly to plants that express several SufE homologues (49), there are two putative SufE-like
163 proteins in *T. gondii* (Table S1), one of which was already predicted to reside in the apicoplast by
164 hyperLOPIT (TgSufE1, TGGT1_239320). We generated a cell line expressing an HA-tagged version of
165 the other, TgSufE2 (TGGT1_277010, Figure S3A, B, C), whose localization was previously unknown.
166 Like for TgSufS, several programs predicted a plastidic transit peptide, which was confirmed by
167 immunoblot analysis (detecting TgSufE2 immature and mature forms, Figure S3D). IFA showed
168 TgSufE2 co-localized with an apicoplast marker (Figure S3E). This further confirms that the initial
169 steps of Fe-S cluster biogenesis in the apicoplast are likely functionally-conserved.

170

171 **Disruption of either the plastidic or the mitochondrial Fe-S cluster pathway has a profound impact**
172 **on parasite growth**

173 In order to get insights into plastidic and mitochondrial Fe-S biogenesis, we generated conditional
174 mutant cell lines in the TgSufS-HA or TgIscU-HA-expressing TATi ΔKu80 background (46).
175 Replacement of the endogenous promoters by an inducible-Tet07*SAG4* promoter, through a single
176 homologous recombination at the loci of interest (Figure S4), yielded conditional TgSufS and TgIscU
177 conditional knock-down cell lines (cKD TgSufS-HA and cKD TgIscU-HA, respectively). In these cell

178 lines, the addition of anhydrotetracycline (ATc) can repress transcription through a Tet-Off system
179 (50). For each cKD cell line several transgenic clones were obtained and found to behave similarly in
180 the initial phenotypic assays we performed, so only one was further analyzed. Transgenic parasites
181 were grown for various periods of time in presence of ATc, and protein down-regulation was
182 evaluated. Immunoblot and IFA analyses of cKD TgSufS-HA and cKD TgIscU-HA parasites showed that
183 the addition of ATc efficiently down-regulated the expression of TgSufS (Figure 3A, C) and TgIscU
184 (Figure 3B, D), and most of the proteins were undetectable after two days of incubation.

185 We also generated complemented cell lines expressing constitutively an additional copy of *TgSufS*
186 and *TgIscU* from the *uracil phosphoribosyltransferase* (*UPRT*) locus from a *tubulin* promoter in their
187 respective conditional mutant backgrounds (Figure S5A, B). We confirmed by semi-quantitative RT-
188 PCR (Figure S5C) that the transcription of *TgSufS* and *TgIscU* qenes was effectively repressed in the
189 cKD cell lines upon addition of ATc, whereas the corresponding complemented cell lines exhibited a
190 high transcription level regardless of ATc addition (due to the expression from the strong *tubulin*
191 promoter).

192 We next evaluated the consequences of TgSufS and TgIscU depletion on *T. gondii* growth in vitro.
193 First, to assess the impact on the parasite lytic cycle, the capacity of the mutants and complemented
194 parasites to produce lysis plaques was analyzed on a host cells monolayer in absence or continuous
195 presence of ATc for 7 days (Figure 4A, B). Depletion of both proteins completely prevented plaque
196 formation, which was restored in the complemented cell lines. To assess whether this defect in the
197 lytic cycle is due to a replication problem, all cell lines were preincubated in ATc for 48 hours and
198 released mechanically, before infecting new host cells and growing them for an additional 24 hours
199 in ATc prior to parasite counting. We noted that incubation with ATc led to an accumulation of
200 vacuoles with fewer parasites, yet that was not the case in the complemented cell lines (Figure 4C,
201 D). Overall, these data show that either TgSufS or TgIscU depletion impacts parasite growth.

202 Then, we sought to assess if the viability of the mutant parasites was irreversibly affected. We thus
203 performed a similar experiment, but at the end of the 7-day incubation, we washed out the ATc,
204 incubated the parasites for an extra 4 days in the absence of the drug and evaluated plaque
205 formation (Figure 4E). In these conditions, while cKD TgSufS-HA parasites displayed very few and very
206 small plaques suggesting their viability was irreversibly impacted, cKD TgIscU-HA parasites showed
207 considerable plaque numbers. However, comparing plaque number between the 7-day and 4-day
208 washout conditions in wells were the same initial dose of cKD TgIscU-HA parasites was added, we
209 could determine that only 28%±2% of plaques were formed after ATc removal (n=3 independent
210 biological replicates), suggesting some mortality.

211 We performed IFAs to assess possible morphological defects that may explain the impaired growths
212 of cKD TgSufS-HA and cKD TgIscU-HA parasites. We stained the apicoplast and mitochondrion of
213 parasites kept in the continuous presence of ATc for several days. cKD TgSufS-HA parasites managed
214 to grow and egress after three days and were seeded onto new host cells, where there were kept for
215 two more days in the presence of ATc. During this second phase of intracellular development, and in
216 accordance with the replication assays (Figure 4C), growth was slowed down considerably. Strikingly,
217 while the mitochondrial network seemed normal, we noticed a progressive loss of the apicoplast
218 (Figure 5A), which was quantified (Figure 5B). The growth kinetics we observed for this mutant are
219 consistent with the "delayed death" effect observed in apicoplast-defective parasites (8, 51, 52). On
220 the other hand, we were able to grow cKD TgIscU-HA parasites for five days of continuous culture:
221 they developed large vacuoles and showed little sign of egress from the host cells (Figure 5C). Both
222 the mitochondrion and the apicoplast appeared otherwise normal morphologically. These large
223 vacuoles could reflect a default in the egress of parasites during the lytic cycle (53). We thus

224 performed an egress assay on cKD TgIscU-HA parasites that were kept for up to five days in the
225 presence of ATc, and they were able to egress normally upon addition of a calcium ionophore (Figure
226 5D). These large vacuoles are also reminiscent of cyst-like structures (54), so alternatively this may
227 reflect spontaneous stage conversion. Cysts are intracellular structures that contain the slow-growing
228 form of *T. gondii*, called the bradyzoite stage (which is responsible for the chronic phase of the
229 disease), and they may appear even during in vitro growth in particular stress conditions (55).

230 In any case, our data show that interfering with the plastidial and mitochondrial Fe-S protein
231 pathways both had important consequences on parasite growth, but had a markedly different impact
232 at a cellular level.

233

234 **Use of label-free quantitative proteomics to identify pathways affected by TgSufS or TgIscU**
235 **depletion**

236 There is a wide variety of eukaryotic cellular processes that are depending on Fe-S cluster proteins.
237 To get an overview of the potential *T. gondii* Fe-S proteome, we used a computational tool able to
238 predict metal-binding sites in protein sequences (56) and performed subsequent manual curation to
239 refine the annotation. We identified 64 proteins encompassing various cellular functions or
240 metabolic pathways that included, beyond the Fe-S synthesis machinery itself, several DNA and RNA
241 polymerases, proteins involved in redox control and electron transfer and radical S-
242 adenosylmethionine (SAM) enzymes involved in methylation and methylthiolation (Table S2).
243 HyperLOPIT data or manual curation helped us assign a putative localization for these canditates. A
244 considerable proportion (19%) of these were predicted to localize to the nucleus, where many
245 eukaryotic Fe-S proteins are known to be involved in DNA replication and repair (57). Yet, strikingly,
246 most of the predicted Fe-S proteins likely localize to the endosymbiotic organelles. Several (19%) are
247 predicted to be apicoplast-resident proteins, including radical SAM enzymes lipoate synthase (LipA)
248 (58) and the MiaB tRNA modification enzyme (59), as well as the IspG and IspH oxidoreductases of
249 the MEP pathway (60). Finally, for the most part (43%) candidate Fe-S proteins were predicted to be
250 mitochondrial, with noticeably several important proteins of the respiratory chain (Fe-S subunit of
251 the succinate dehydrogenase complex, Rieske protein and TgApiCox13) (61–63), but also enzymes
252 involved in other metabolic pathways such as heme or molybdopterin synthesis. CRISPR/Cas9 fitness
253 scores (43) confirmed many of these putative Fe-S proteins likely support essential functions for
254 parasite growth.

255 We sought to confirm these results experimentally. Thus, in order to uncover the pathways primarily
256 affected by the depletion of TgIscU and TgSufS, and to identify potential Fe-S protein targets, we
257 conducted global label free quantitative proteomic analyses. Like most plastidic or mitochondrial
258 proteins, candidate Fe-S acceptors residing in these organelles are nuclear-encoded and thus need to
259 be imported after translation and have to be unfolded to reach the stroma of the organelle. This not
260 only implies the addition of the Fe-S cofactor should happen locally in the organelle, but also that this
261 may have a role in proper folding of these proteins. We thus assumed that disrupting a specific
262 pathway may have a direct effect on the stability and expression levels of local Fe-S proteins. Cellular
263 downstream pathways or functions may also be affected, while other pathways may be upregulated
264 in compensation. Parasites were treated for two days with ATc (TgIscU-HA) or three days (cKD
265 TgSufS-HA, as it takes slightly longer to be depleted, Figure 3A) prior to a global proteomic analysis
266 comparing protein expression with the ATc-treated TATi ΔKu80 control. For each mutant, we
267 selected candidates with a log2(fold change) ≤-0.55 or ≥0.55 (corresponding to a ~1.47 fold change in
268 decreased or increased expression) and a p-value <0.05 (ANOVA, *n*=4 biological replicates) (Tables S3

269 and S4, Figure 6A). To get a more exhaustive overview of proteins whose amounts varied drastically,
270 we completed this dataset by selecting some candidates that were consistently and specifically
271 absent from the mutant cell lines or only expressed in these (Tables S3 and S4).

272 Overall, depletion of TgIscU led to a higher variability in protein expression and while the pattern of
273 expression was essentially specific for the respective mutants, a number of shared variant proteins
274 were found (Figure 6B, Table S5). For instance, common lower expressed candidates include a SAM
275 synthase, possibly reflecting a general perturbation of SAM biosynthesis upon loss of function of Fe-
276 S-containing radical SAM enzymes (64). Using dedicated expression data (65, 66) available on
277 ToxoDB.org we realized that, strikingly, many of the common variant proteins were stage-specific
278 proteins (Table S5). For instance, the protein whose expression went down the most is SAG-related
279 sequence (SRS) 19F. The SRS family contains GPI-anchored surface antigens related to SAG1, the first
280 characterized *T. gondii* surface antigen, and whose expression is largely stage-specific (67). This
281 protein, SRS19F is expressed in bradyzoites, but may be most highly expressed in stages present in
282 the definitive host (66, 68). Conversely, SRS44, also known as CST1 and one of the earliest marker of
283 stage conversion to bradyzoites (69), was upregulated in both mutants. Several other bradyzoite
284 proteins whose expression increased included Ank1, a tetratricopeptide-repeat protein highly
285 upregulated in the cyst-stages but not necessary for stage conversion (70), aspartyl protease ASP1,
286 an α-galactosidase, as well as several dense granule proteins (GRA). Dense granules are specialized
287 organelles that secrete GRA proteins that are known to participate in nutrient acquisition, immune
288 evasion, and host cell-cycle manipulation. Many GRA have been characterized in the tachyzoite
289 stage, but several stage-specific and expressed in bradyzoites (71). It should be noted that
290 bradyzoite-specific proteins were generally much strongly expressed upon TgIscU depletion than
291 TgSufS depletion. Nevertheless, altogether these results show that altering either the plastidic or the
292 mitochondrial Fe-S cluster synthesis pathway led to an initial activation of the expression of some
293 markers of the bradyzoite stage, whose involvement in the stress-mediated response is well
294 documented (55).

295

296 **Depletion of TgSufS has an impact on the apicoplast, but also beyond the organelle**

297 We next focused on proteins that varied upon depletion of TgSufS (Table S3). Using the hyperLOPIT
298 data available on ToxoDB.org, we assessed the putative localization of the candidates (Figure 7A) and
299 we also defined putative functional classes based on manual curation (Figure 7B). Surprisingly, few
300 apicoplast proteins were impacted. This could reflect a limited impact on apicoplast Fe-S
301 apoproteins, but this is in contradiction with the strong and specific effect we see on the organelle in
302 the absence of TgSufS (Figure 5A, B). There might also be a bias due to an overall low protein
303 abundance: less than half of the apicoplast candidates of the predicted Fe-S proteome (Table S2)
304 were robustly detected even in the control for instance, including our target protein SufS. Finally, of
305 course it is possible that depletion of Fe-S clusters, while impacting the functionality of target
306 proteins, did not have a considerable effect on their abundance. We sought to verify this for
307 apicoplast stroma-localized LipA, a well-established and evolutionarily-conserved Fe-S cluster
308 protein, which was found to be only marginally less expressed in our analysis (Table S3). LipA is
309 responsible for the lipoylation of a single apicoplast target protein, the E2 subunit of the pyruvate
310 dehydrogenase (PDH) (37). Using an anti-lipoic acid antibody on cKD TgSufS-HA protein extracts, we
311 could already see a marked decrease in lipoylated PDH-E2 after only one day of ATc incubation
312 (Figure 7C). This was not due to a general demise of the apicoplast as it considerably earlier than the
313 observed loss of the organelle (Figure 5A, B), and levels of the CPN60 apicoplast marker were clearly

314 not as markedly impacted (Figure 7C). This finding confirmed apicoplast Fe-S-dependent activities are
315 specifically affected in our mutant, before observing the general demise and loss of the organelle.

316 Other potential apicoplast Fe-S cluster-containing proteins include IspG and IspH, key enzymes of the
317 MEP isoprenoid synthesis pathway (60). Again, these proteins were only found marginally less
318 expressed in our quantitative analysis, yet our proteomics dataset provided indirect clues that their
319 function may be impacted. Isoprenoids precursors can be used as lipophilic groups to modify
320 proteins, but may also be incorporated into lipids like ubiquinone, which is an important
321 polyprenylated cofactor of the mitochondrial respiratory chain. Quite strikingly, a single predicted
322 mitochondrial candidate was significantly less expressed upon TgSufS depletion and is homolog of
323 the UbiE/COQ5 methyltransferase, which is involved in ubiquinone synthesis (72). Isoprenoids are
324 also important for dolichol-derived protein glycosylation and glycosylphosphatidylinositol (GPI)-
325 anchor biosynthesis. That may account for effects of TgSufS depletion on specific proteins. For
326 instance, the three potentially rhoptry-localized candidates significantly less expressed (Table S3) are
327 predicted to be GPI-anchored and/or glycosylated. Overall, this might be an indication that TgSufS
328 depletion impacts isoprenoid synthesis in the apicoplast, which in turn would impact other metabolic
329 pathways.

330 There were additional indications that TgSufS depletion has consequences beyond apicoplast
331 metabolism, as we noticed clear variations in other proteins residing in other subcellular
332 compartments. For instance, changes in expression of stage-specific GRA and SRS proteins reflecting,
333 as mentioned before, a possible initiation of stage conversion to bradyzoites. Interestingly, the higher
334 expression of Golgi apparatus/plasma membrane transporters or endoplasmic reticulum (ER)-located
335 lipid-related enzymes suggest some sort of metabolic adaptation occurs upon depletion of TgSufS
336 (Figure 7A, B). The apicoplast and the ER cooperate for fatty acid (FA) and phospholipid (PL) synthesis
337 (73). The apicoplast generates short FA chains through the FASII system, but also lysophosphatidic
338 acid (LPA) as a PL precursor (74), and FA chains can then be further modified by ER-localized enzymes
339 that include elongases. Yet, these the ER-localized PL-synthesis machinery can also use FA scavenged
340 from the host (75). The increased expression of ER-localized lipid-related enzymes may thus reflect
341 an increased synthesis, potentially from exogenous lipid precursors, in compensation from a defect
342 in the apicoplast-localized machinery. Overall, this suggests impacting the Fe-S cluster synthesis
343 pathway in the apicoplast had important metabolic consequences beyond the organelle itself.

344

345 **Depletion of TgIscU impacts the respiratory capacity of the mitochondrion and leads to stage**
346 **conversion**

347 We also analyzed the proteins whose abundance changed upon TgIscU depletion (Table S4). Again,
348 we used hyperLOPIT data to determine the localization of variant proteins (Figure 8A) and we also
349 inferred their potential function from GO terms or manual curation (Figure 8B). Depletion of TgIscU
350 had a notable impact locally, as numerous mitochondrial proteins were found in lower abundance.
351 Remarkably, most of these proteins were identified as members of the mitochondrial respiratory
352 chain. This ETC comprises five complexes, in which several Fe-S proteins have important function. As
353 mentioned earlier, they include the iron-sulfur subunit of the succinate dehydrogenase complex
354 (complex II), the Rieske protein (part of complex III, with cytochrome *b* and *c*1) and TgApiCox13 (part
355 of complex IV, the cytochrome *c* oxidase) (61–63). Not only these three Fe-S cluster proteins were
356 found to be less expressed upon TgIscU depletion, but most components of the complexes III and IV
357 (including recently characterized parasite-specific subunits (62, 63)) were also significantly less
358 abundant (Table S4). This suggested the mitochondrial membrane potential and consequently the

359 respiratory capacity of the mitochondrion were likely altered in the absence of a functional
360 mitochondrial Fe-S cluster synthesis pathway. To verify this, we performed flow cytometry
361 quantification using JC-1, a monomeric green fluorescent carbocyanine dye that accumulates as a red
362 fluorescent aggregates in mitochondria depending on their membrane potential (Figure 9A).
363 Depletion of TgIscU led to a marked decrease of the parasite population displaying a strong red signal
364 (Figure 9B). The effect was maximal after two days of ATc treatment and not further increased by a
365 four-day treatment, which is consistent with the quantitative proteomics data already showing
366 strong impact on proteins from complexes II, III and IV after only two days of ATc treatment.
367 Concomitantly to the lesser expression of mitochondrial respiratory chain subunits, the proteomics
368 analysis revealed TgIscU depletion induced a significant increase in cytosolic enzymes involved in
369 glycolysis, as well as its branching off pentose phosphate pathway (Figure 8A, B, Table S4). The
370 upregulation of glycolytic enzymes potentially reflects a metabolic compensation for mitochondrial
371 defects in energy production due to the impairment of the respiratory chain. Other proteins whose
372 abundance was markedly decreased were predicted to cytoplasmic or nuclear, which is perhaps
373 unsurprising as the cytosolic CIA Fe-S cluster assembly pathway is supposedly dependent from the
374 SUF pathway (29). The changes in abundance of several RNA-binding proteins involved in mRNA half-
375 life or transcription/translation regulation may also reflect adaptation to a stress.

376 Indeed, another feature highlighted by the quantitative proteomics analysis of the TgIscU mutant is
377 the change in the expression of stage-specific proteins (Table S4). The expression of several
378 bradyzoite-specific including GRAs and proteins of the SRS family, was strongly increased. At the
379 same time, some tachyzoite-specific SRS and GRA proteins were found to be less expressed. This was
380 supporting the idea that intracellularly developing parasites lacking TgIscU may convert into bona
381 fide cyst-contained bradyzoites, as suggested by our initial morphological observations (Figure 5C).
382 To verify this, we used a lectin from the plant *Dolichos biflorus*, which recognizes the SRS44/CST1
383 glycoprotein that is exported to the wall of differentiating cysts (69). We could see that during
384 continuous growth of cKD TgIscU-HA parasites in the presence of ATc, there was an increasing
385 number of DBL-positive structures (Figure 10A). This was quantified during the first 48 hours of
386 intracellular development (Figure 10B) and, interestingly, was shown to mimic the differentiation
387 induced by nitric oxide, a known factor of stage conversion (76), and a potent damaging agent of Fe-S
388 clusters (77). We combined RNAseq expression data for tachyzoite and bradyzoite stages (66) to
389 establish a hierarchical clustering of the SRS proteins detected in our quantitative proteomics
390 experiments for the two mutants (Figure 10C). This clearly confirmed a strong increase in the
391 expression of bradyzoite-specific SRS in the TgIscU mutant. As mentioned earlier, some were also
392 upregulated in the TgSufS mutant but in much lesser proportions. The strongest increase in
393 bradyzoite-specific SRS expression upon TgSufS depletion was for SRS44/CST1, which happens to be
394 the protein DBL preferentially binds to (69). However, contrarily to the TgIscU mutant, labelling
395 experiments did not indicate any detectable increase in DBL recruitment in the TgSufS mutant (Figure
396 10B), confirming that impairing the plastidic Fe-S center synthesis pathway does not trigger full stage
397 conversion in this cell line. Stage conversion is a progressive process that happens over the course of
398 several days, as it involves the expression of distinct transcriptomes and proteomes (55). Markers for
399 specific steps of in vitro cyst formation had been previously described (78), so we have used several
400 of these to check the kinetics of stage conversion in the TgIscU-depleted parasites. We kept the cKD
401 TgIscU-HA parasites for up to 20 days in the presence of ATc and tested for the presence of SAG1
402 (tachyzoite maker), DBL (early bradyzoite marker), P18/SAG4 (intermediate bradyzoite marker) and
403 P21 (late bradyzoite marker) (Figure 10D). After 7 days of ATc treatment, the DBL-positive cyst
404 contained parasites were still expressing SAG1 and not yet SAG4, whereas after 20 days parasites
405 with SAG4 labelling were found, but there was still a residual SAG1 expression; expression of late

406 marker P21 was, however, never detected. This suggests stage conversion of these parasites
407 progresses beyond the appearance of early cyst wall markers, but not only it does so with slow
408 kinetics, but it seems incomplete. In fact, observation of DBL-positive cysts showed a marked
409 decrease in their mean size between the 7 and 20 days timepoints (Figure 10D). This suggests
410 incomplete conversion may be leading to subsequent reactivation/reinvasion events. There is also
411 possibly a lack of fitness in the long term for the TgIscU-depleted converting parasites, which would
412 be in accordance with our plaque assays that showed not all mutant parasites were able to grow
413 back upon ATc removal.

414

415 **Discussion**

416 Because of their origin and metabolic importance, the two apicomplexan endosymbiotic organelles
417 have gathered considerable interest as potential drug targets (79, 80). It may be obvious as for
418 example the plastid hosts several metabolic pathways which are not present in the mammalian hosts
419 of these parasites. Yet, even for conserved housekeeping functions or, in the case of the
420 mitochondrion early phylogenetic divergence, may still provide enough molecular differences to
421 allow selective chemical inhibition. In fact, several drugs used for prophylactic or curative treatments
422 against Apicomplexa-caused diseases are already targeting these organelles. They are essentially
423 impacting the organellar protein synthesis by acting on the translation machinery (81), although the
424 mitochondrial respiratory chain inhibitor atovaquone is also used to treat malaria and toxoplasmosis
425 (82). One main difference when targeting *Plasmodium* and *Toxoplasma* by drugs is that the latter
426 easily converts into the encysted bradyzoite resistance form. It has been known for some time that
427 treatment of tachyzoites with mitochondrial inhibitors triggers stage conversion (76, 83, 84). This
428 may be efficient to counteract the acute phase of toxoplasmosis, but at the same time may favour
429 persistence of the parasites in the host.

430 Here we characterized pathways which are very similar biochemically, but are located into two
431 distinct endosymbiotic organelles and whose inactivation has drastically different effects on the
432 parasites. Fe-S clusters are ancient, ubiquitous and fundamental to many cellular functions, but their
433 synthesis by distinct biosynthetic pathways was inherited by specific endosymbiotic organelles
434 through distinct bacterial ancestors, and have thus specialized into adding these cofactors to
435 different client proteins (27). A key function of Fe-S clusters, owing to their mid-range redox
436 potential, is electron transfer and redox reactions, mainly as components the respiratory and
437 photosynthetic electron transfer chains. They also have important functions in stabilizing proteins,
438 redox sensing, or catalysis through SAM enzymes. Several of these are not retained in Apicomplexa,
439 whose plastid has lost its photosynthetic ability for example. Nevertheless, our prediction of the *T.*
440 *gondii* Fe-S proteins repertoire suggests many key functions associated with the apicoplast or the
441 mitochondrion are likely to be affected by a perturbation of Fe-S assembly (Table S2).

442 For the apicoplast, these include lipoic acid or isoprenoid synthesis. Inactivation of the apicoplast-
443 located TgSufS had a marked effect on the organelle itself, as it led ultimately to a loss of the
444 apicoplast, which is consistent with the phenotype observed when disrupting the Suf pathway in
445 *Plasmodium* (31). Isoprenoid synthesis is vital for *T. gondii* tachyzoites (38), and it has implication
446 beyond the apicoplast, as prenylated proteins or isoprenoid precursors are involved in more general
447 cellular processes including intracellular trafficking or mitochondrial respiration (85). Impairing
448 isoprenoid synthesis does not, however, necessarily lead to a loss of the organelle (31). There may
449 thus be another explanation for this phenotype. Interestingly, we could show that perturbing the Suf
450 pathway, which is supposedly important for Fe-S-containing enzyme LipA, impacts the lipoylation of

451 E2 subunit of the apicoplast-located PDH (Figure 7C). The PDH complex catalyzes the production of
452 acetyl-CoA, which is the first step of the FASII system, and perturbation of either the PDH or other
453 steps of the FASII system lead to a loss of the organelle and severely impairs fitness of the parasites
454 (38, 86). Our quantitative proteomic analysis shows potential compensatory mechanisms may be
455 used by the parasites in response this early perturbation of the apicoplast lipid metabolism that
456 precedes organelle loss. Tachyzoites are indeed known to be able to use exogenous lipid sources to
457 adapt metabolically (86, 87), and interestingly upon depletion of TgSufS we observed a pattern of
458 overexpression for ER-located enzymes involved in the synthesis of several phospholipids and
459 ceramides (Table S3). These lipids are usually synthesized in the ER from apicoplast-synthesized
460 precursors, but this may clearly indicate a compensatory mechanism that would make use of
461 precursors scavenged form the host instead. In spite of this, it seems the alteration of the Suf
462 pathway in *T. gondii* has such a profound impact on the apicoplast itself, that is causes a typical
463 "delayed death" phenotype that ultimately leads to the irreversible demise of the parasites (Figure
464 4).

465 For the mitochondrion, important pathways potentially involving Fe-S proteins include the
466 respiratory ETC, the TCA cycle, as well as molybdenum and heme synthesis (Table S2). Accordingly,
467 perhaps the most obvious consequence of disrupting the ISC pathway was the profound impact on
468 the mitochondrial respiratory capacity, as evidenced experimentally by measuring the mitochondrial
469 membrane potential (Figure 9), and supported by proteomic analyses showing a clear drop in
470 expression of many respiratory complex proteins (Table S4). Although the mitochondrion, through
471 the TCA cycle and the respiratory chain/oxidative phosphorylation, contributes to energy production
472 in tachyzoites (88), the glycolytic flux is also believed to be a major source of carbon and energy for
473 these parasites (89). Thus, rather coherently, as highlighted by our quantitative proteomic analysis,
474 disruption of the ISC pathway led to the overexpression of glycolytic enzymes concurrently with the
475 lower expression of mitochondrial ETC components. The overexpression of enzymes of the pentose
476 phosphate pathway, which is branching off from glycolysis and is providing redox equivalents and
477 precursors for nucleotide and amino acid biosynthesis, is also potentially indicative of a higher use of
478 glucose in these conditions. The metabolic changes encountered by SUF-deficient parasites do not
479 cause their rapid demise, as they are able to initiate conversion to the bradyzoite stage, which has
480 been suggested to rely essentially on glycolysis for energy production anyway (90).

481 The transition from tachyzoite to bradyzoite is known to involve a considerable change in gene
482 expression (65, 66), and it takes several days of in vitro differentiation-inducing conditions to obtain
483 mature cysts (91, 92). TgIscU-depleted parasites rapidly displayed a high expression of bradyzoite-
484 specific surface antigens and GRA markers (Table S4, Figure 10), and as they developed they were
485 included in structures with typical cyst-like morphology (Figure 5, Figure 10). However, using specific
486 antibodies against early or late bradyzoite markers, we could see that even when depleting TgIscU
487 for an extended time period, the differentiating parasites never appeared to reach fully mature
488 bradyzoite stage (Figure 10). One of the reason is that our mutants were generated in a type I *T.*
489 *gondii* strain, which is associated with acute toxoplasmosis in the mouse model (93) and typically
490 does not form cysts: type I tachyzoites may upregulate specific bradyzoite genes and, according to
491 some reports, produce bradyzoite-specific proteins or cyst wall components, but are largely
492 incapable of forming mature bradyzoite cysts (94). A second explanation is that these parasites may
493 not be viable long enough to fully differentiate. For instance, although we found the impact of TgIscU
494 depletion on the lytic cycle was partly reversible, a large proportion of the parasites was not able to
495 recover after 7 days of ATc treatment. This may not be solely due to the alteration of the
496 mitochondrial metabolism, as the inactivation of the ISC pathway likely has consequences on other
497 important cellular housekeeping functions. In other eukaryotes, the SUF pathway provides a yet

498 unknown precursor molecule as a sulfur provider for the cytosolic CIA Fe-S cluster assembly pathway
499 (29). The ISC pathway thus not only governs the proper assembly of mitochondrial Fe-S proteins, but
500 also of cytoplasmic and nuclear ones. Our quantitative proteomics data suggests it is also the case in
501 *T. gondii*, as several putative nuclear Fe-S proteins involved in gene transcription (such as DNA-
502 dependent RNA polymerases) or DNA repair (like DNA endonulease III) were found to be impacted by
503 TgIscU depletion. The CIA pathway has recently been shown to be important for tachyzoite
504 proliferation (30), and several of the cytoplasmic or nuclear Fe-S cluster-containing proteins are likely
505 essential for parasite viability. It is thus possible that in spite of their conversion to a stress-resistant
506 form, the long-term viability of TgIscU parasites could be affected beyond recovery.

507 Our quantitative proteomics analysis shows that SUF-impaired parasites also seem to initiate an
508 upregulation of some bradyzoite markers early after TgSufS depletion. Yet, these parasites did not
509 display the hallmarks of bradyzoite morphology. They did not progress towards stage conversion and
510 instead they eventually died. Both the apicoplast and the mitochondrion have established a close
511 metabolic symbiosis with their host cell, so there are likely multiple mechanisms allowing these
512 organelles to communicate their status to the rest of the cell. This raises the question as to why
513 mitochondrion, but not apicoplast, dysfunction can lead to differentiation into bradyzoites. This may
514 be due to differences in the kinetics or the severity of apicoplast-related phenotypes that may not
515 allow stage conversion (which is typically a long process) to happen. Alternatively, there might be
516 differentiation signals specifically associated to the mitochondrion. In fact this organelle is
517 increasingly seen as a signalling platform, able to communicate its fitness through the release of
518 specific metabolites, reactive oxygen species, or by modulating ATP levels (95). Interestingly, it was
519 shown in other eukaryotes that mitochondrial dysfunctions such as altered oxidative phosphorylation
520 significantly impair cellular proliferation, oxygen sensing or specific histone acetylation, yet without
521 diminishing cell viability and instead may lead to quiescent states (96, 97). Environmental and
522 metabolic cues likely drive specific gene expression, leading to a functional shift to drive stage
523 conversion, but how are these stimuli integrated is largely unknown. A high-throughput approach has
524 allowed the recent identification of a master transcriptional regulator of stage conversion (98), but
525 how upstream events are converted into cellular signals to mobilize the master regulator is still an
526 important, yet unresolved, question. Translational control (99) may play a role in regulating this
527 factor in the context of the integrated stress response (100). In fact, an essential part of the
528 eukaryotic cell stress response occurs post-transcriptionally and is achieved by RNA-binding proteins
529 (101). Interestingly, among the proteins significantly less abundant in the mitochondrial SUF pathway
530 mutant were many RNA-binding proteins, including components of stress granules (PolyA-binding
531 protein, PUF1, Alba1 and 2, some of which are linked to stage conversion (102–104)) which are
532 potentially involved in mRNA sequestration from the translational machinery, but also two regulators
533 of the large 60S ribosomal subunit assembly, as well as the gamma subunit of the eukaryotic
534 translation initiation factor (eIF) complex 4 (known to be down-regulated in the bradyzoite stage
535 (105)). Variation in these candidates may have a considerable impact on the translational profile and
536 on the proteostasis of differentiating parasites, and how they may help regulating stage conversion
537 in this context should be investigated further. Understanding the mechanisms that either lead to
538 encystment or death of the parasites is crucial to the development of treatments against
539 toxoplasmosis. This question is key to the pathology caused by *T. gondii*, as bradyzoites act as
540 reservoirs susceptible to reactivate as and cause acute symptoms, and are essentially resistant to
541 treatment. Comparative studies of stress-induced or spontaneously differentiating conditional
542 mutants may bring further insights on how the parasites integrate upstream stresses or dysfunctions
543 into global regulation of stage conversion.

544

545

546 **Materials and methods**

547 **Parasites and cells culture.** Tachyzoites of the TATi ΔKu80 *T. gondii* strain (46), as well as derived
548 transgenic parasites generated in this study, were maintained by serial passage in human foreskin
549 fibroblast (HFF, American Type Culture Collection, CRL 1634) cell monolayer grown in Dulbecco's
550 modified Eagle medium (Gibco), supplemented with 5% decomplemented fetal bovine serum, 2-mM
551 L-glutamine and a cocktail of penicillin-streptomycin at 100 µg/ml.

552 **Bioinformatic analyses.** Sequence alignments were performed using the MUltiple Sequence
553 Comparison by Log-Expectation (MUSCLE) algorithm of the Geneious 6.1.8 software suite
554 (http://www.geneious.com). Transit peptide and localization predictions were done using IPSORT
555 (http://ipsort.hgc.jp/), Localizer 1.0.4 (http://localizer.csiro.au/), and Deeploc 1.0
556 (http://www.cbs.dtu.dk/services/DeepLoc-1.0/) algorithms.

557 The putative Fe-S proteome was predicted using the MetalPredator webserver
558 (http://metalweb.cerm.unifi.it/tools/metalpredator/) (56). The whole complement of *T. gondii*
559 annotated proteins was downloaded in FASTA format from the ToxoDB database (https://toxodb.org
560 (41), release 45) and used for analysis in the MetalPredator webserver. Additional manual curation
561 included homology searches for known Fe-S proteins from plants (see appendix A in (106)), and
562 search for homologues in the Uniprot database (https://www.uniprot.org) that were annotated as
563 containing a Fe-S cofactor. For proteomics candidates, annotations were inferred from ToxoDB,
564 KEGG (https://www.genome.jp/kegg/)
565 and the Liverpool Library of Apicomplexan Metabolic Pathways (http://www.llamp.net/ (107)).
566 N-glycosylation predictions were done with the GlycoEP webserver
567 (http://crdd.osdd.net/raghava/glycoep/index.html). GPI anchor predictions were done with the
568 PredGPI (http://gpcr.biocomp.unibo.it/predgpi/) and GPI-SOM (http://gpi.unibe.ch/) webservers.

569 **Heterologous expression in *E. coli*.** Constructs for designing recombinant proteins were defined by
570 aligning TgSufS and TgIscU amino acid sequences with their *E. coli* counterparts. For *TgSufS*, a 1,438
571 bp fragment corresponding to amino acids 271-699, was amplified by polymerase chain reaction
572 (PCR) from *T. gondii* cDNA using primers ML4201/ML4012 (sequences of the primers used in this
573 study are found in Table S6). For *TgIscU*, a 393 bp fragment corresponding to amino acids 64-194,
574 was amplified by PCR from *T. gondii* cDNA using primers ML4204/ML4205. The fragments were
575 cloned into the pUC19 (Thermo Fisher Scientific) using the HindIII/BamHI and SphI/BamHI restriction
576 sites, respectively. *E. coli* mutants from the Keio collection (obtained from the The *Coli* Genetic Stock
577 Center at the University of Yale: stain numbers JW1670-1 for *SufS*, JW2513-1 for *IscU*), were
578 transformed with plasmids for expressing recombinant TgSufS and TgIscU and selected with
579 ampicillin. For growth assays (108), overnight stationary phase cultures were adjusted to the same
580 starting OD_{600} of 0.6 in salt-supplemented M9 minimal media containing 0.4% glucose and varying
581 amounts of the 2,2′-Bipyridyl iron chelator (Sigma-Aldrich). Growth was monitored through OD_{600}
582 measurement after 7, 14 and 24 hours at 37°C in a shaking incubator.

583 **Generation of HA-tagged TgSufS, TgSufE2 and TgIscU cell lines.** The ligation independent strategy
584 (45) was used for C-terminal hemagglutinin $(HA)_3$-tagging TgIscU. Fragment corresponding to the 3'
585 end of the target gene was amplified by PCR from genomic DNA, with the Q5 DNA polymerase (New
586 England BioLabs) using primers ML4208/ML4209 (*TgIscU*) and inserted in frame with the sequence
587 coding for a triple HA tag, present in the pLIC-HA_3-chloramphenicol acetyltransferase (CAT) plasmid.
588 The resulting vector was linearized and 40 µg of DNA was transfected into the TATi ΔKu80 cell line to

589 allow integration by single homologous recombination, and transgenic parasites of the TgIscU-HA cell
590 line were selected with chloramphenicol and cloned by serial limiting dilution.

591 For TgSufS and TgSufE2, a CRISPR-based strategy was used. Using the pLIC-HA_3-CAT plasmid as a
592 template, a PCR was performed with the KOD DNA polymerase (Novagen) to amplify the tag and the
593 resistance gene expression cassette with primers ML3978/ML3979 (*TgSufS*) and ML4023/ML4162
594 (*TgSufE2*), that also carry 30 bp homology with the 3 end of the corresponding genes. A specific
595 single-guide RNA (sgRNA) was generated to introduce a double-stranded break at the 3 of the
596 respective loci. Primers used to generate the guides were ML3948/ML3949 (*TgSufS*) and
597 ML4160/ML4161 (*TgSufE2*) and the protospacer sequences were introduced in the Cas9-expressing
598 pU6-Universal plasmid (Addgene, ref #52694) (43). Again, the TATi ΔKu80 cell line was transfected
599 and transgenic parasites of the TgSufS-HA or TgSufE2-HA cell lines were selected with
600 chloramphenicol and cloned by serial limiting dilution.

601 **Generation of TgSufS and TgIscU conditional knock-down and complemented cell lines.** The
602 conditional knock-down cell for *TgSufS* and *TgIscU* were generated based on the Tet-Off system using
603 the DHFR-TetO7Sag4 plasmid (109).

604 For *TgIscU*, a 930 bp 5' region of the gene, starting with the initiation codon, was amplified from
605 genomic DNA by PCR using Q5 polymerase (New England Biolabs) with primers ML4212/ML4213 and
606 cloned into the DHFR-TetO7Sag4 plasmid, downstream of the anhydrotetracycline (ATc)-inducible
607 TetO7Sag4 promoter, obtaining the DHFR-TetO7Sag4-TgIscU plasmid. The plasmid was then
608 linearized and transfected into the TgIscU-HA cell line. Transfected parasites were selected with
609 pyrimethamine and cloned by serial limiting dilution.

610 For *TgSufS*, a CRISPR-based strategy was used. Using the DHFR-TetO7Sag4 plasmid as a template, a
611 PCR was performed with the KOD DNA polymerase (Novagen) to amplify the promoter and the
612 resistance gene expression cassette with primers ML4154/ML4155 that also carry 30 bp homology
613 with the 5 end of the *TgSufS* gene. A specific single-guide RNA (sgRNA) was generated to introduce
614 a double-stranded break at the 5 of the *TgSufS* locus. Primers used to generate the guide were
615 ML4156/ML4157 and the protospacer sequences were introduced in the pU6-Universal plasmid
616 (Addgene ref#52694) (43). The TgSufS-HA cell line was transfected with the donor sequence and the
617 Cas9/guide RNA-expressing plasmid and transgenic parasites were selected with pyrimethamine and
618 cloned by serial limiting dilution.

619 The cKD TgSufS-HA and cKD TgIscU-HA cell lines were complemented by the addition of an extra copy
620 of the respective genes put under the dependence of a tubulin promoter at the *uracil*
621 *phosphoribosyltransferase* (*UPRT*) locus. *TgSufS* (2097 bp) and *TgIscU* (657 bp) whole cDNA
622 sequences were amplified by reverse transcription (RT)-PCR with primers ML4576/ML4577 and
623 ML4455/ML4456, respectively. They were then cloned downstream of the *tubulin* promoter
624 sequence of the pUPRT-TUB-Ty vector (46) to yield the pUPRT-TgSufS and pUPRT-TgIscU plasmids,
625 respectively. These plasmids were then linearized prior to transfection of the respective mutant cell
626 lines. The recombination efficiency was increased by co-transfecting with the Cas9-expressing pU6-
627 UPRT plasmids generated by integrating *UPRT*-specific protospacer sequences (with primers
628 ML2087/ML2088 for the 3' and primers ML3445/ML3446 for the 5') which were designed to allow a
629 double-strand break at the *UPRT* locus. Transgenic parasites were selected using
630 5-fluorodeoxyuridine and cloned by serial limiting dilution to yield the cKD TgSufS-HA comp cKD
631 TgIscU-HA comp cell lines, respectively.

632 **Immunoblot analysis.** Protein extracts from 10^7 freshly egressed tachyzoites were prepared in
633 Laemmli sample buffer, separated by SDS-PAGE and transferred onto nitrocellulose membrane using

634 the BioRad Mini-Transblot system according to the manufacturer's instructions. Rat monoclonal
635 antibody (clone 3F10, Roche) was used to detect HA-tagged proteins. Other primary antibodies used
636 were rabbit anti-lipoic acid antibody (ab58724, Abcam), mouse anti-SAG1 (110), rabbit anti-CPN60
637 (111) and mouse anti-actin (112).

638 **Immunofluorescence microscopy.** For immunofluorescence assays (IFA), intracellular tachyzoites
639 grown on coverslips containing HFF monolayers, were either fixed for 20 min with 4% (w/v)
640 paraformaldehyde in PBS and permeabilized for 10 min with 0.3% Triton X-100 in PBS or fixed for
641 5 min in cold methanol (for the use of cyst-specific antibodies). Slides/coverslips were subsequently
642 blocked with 0.1% (w/v) BSA in PBS. Primary antibodies used (at 1/1,000, unless specified) to detect
643 subcellular structures were rabbit anti-CPN60 (111), mouse monoclonal anti-F1-ATPase beta subunit
644 (gift of P. Bradley), mouse monoclonal anti-GRA3 (113), rabbit anti-GAP45 (114), mouse monoclonal
645 anti-SAG1 (110), anti SAG4/P18 (diluted 1/200, T8 3B1) and anti P21 (diluted 1/200, T8 4G10) (115).
646 Rat monoclonal anti-HA antibody (clone 3F10, Roche) was used to detect epitope-tagged proteins.
647 Staining of DNA was performed on fixed cells by incubating them for 5 min in a 1 µg/ml
648 4,6-diamidino-2-phenylindole (DAPI) solution. All images were acquired at the Montpellier RIO
649 imaging facility from a Zeiss AXIO Imager Z1 epifluorescence microscope driven by the ZEN software
650 v2.3 (Zeiss). Z-stack acquisition and maximal intensity projection was performed to visualize larger
651 structures such as in vitro cysts. Adjustments for brightness and contrast were applied uniformly on
652 the entire image.

653 **Plaque assay.** Confluent monolayers of HFFs were infected with freshly egressed parasites, which
654 were left to grow for 7 days in the absence or presence of ATc. They were then fixed with 4% v/v
655 paraformaldehyde (PFA) and plaques were revealed by staining with a 0.1% crystal violet solution
656 (V5265, Sigma-Aldrich).

657 **Egress assay.** *T. gondii* tachyzoites were grown for 40 (without ATc) or 120 (with ATc) hours on HFF
658 cells with coverslips in 24-well plates. The infected host cells were incubated for 7 min at 37°C with
659 DMEM containing 3 µM of calcium ionophore A23187 (C7522, Sigma-Aldrich) prior to fixation with
660 4% PFA. Immunofluorescence assays were performed as previously described (116): the parasites
661 and the parasitophorous vacuole membrane were labelled with anti-GAP45 and anti-GRA3,
662 respectively. The proportion of egressed and non-egressed vacuoles was calculated by counting 250
663 vacuoles in three independent experiments. Data are presented as mean values ± SEM.

664 **Semi-quantitative RT-PCR.** Total mRNAs of freshly egressed extracellular parasites from the cKD
665 TgSufS-HA, cKD TgIscU-HA and their respective complemented cell lines (incubated with or without
666 ATc at 1.5 µg/mL for 3 days) were extracted using Nucleospin RNA II Kit (Macherey-Nagel). The
667 cDNAs were synthesized with 450 ng of total RNA per RT-PCR reaction using High-Capacity cDNA
668 Reverse Transcription Kit (Applied Biosystems). Specific primers for *TgSufS* (ML4686/ML4687), *TgIscU*
669 (ML4684/ML4685) and, as a control, *Tubulin β* (ML841/ML842) were used to amplify specific
670 transcripts with the GoTaq DNA polymerase (Promega). PCR was performed with 21 cycles of
671 denaturation (30 s, 95 °C), annealing (20 s, 55 °C), and elongation (30 s, 72 °C).

672 **Mitochondrial membrane potential measurement.** Parasites grown for the indicated time with or
673 without ATc were mechanically released from their host cells, purified on a glass wool fiber column,
674 washed and adjusted to 10^7 parasites/ml in phenol red-free medium, and incubated in with 1.5 µM
675 of the JC-1 dye (5,5',6,6'-tetrachloro-1,1',3,3'-tetraethylbenzimidazolylcarbocyanine Iodide, T3168,
676 Invitrogen) for 30 min at 37°C, washed phenol red-free medium and analyzed by flow cytometry or
677 microscopy. Flow cytometry analysis was performed on a FACSAria III flow cytometer (Becton

678 Dickinson). An unstained control was used to define gates for analysis. 50,000 events per condition
679 were collected and data were analysed using the FlowJo Software.

680 **Quantitative label-free mass spectrometry.** Parasites of the TATi ΔKu80 and cKD TgIscU-HA cell lines
681 were grown for two days in the presence of ATc; parasites of the cKD TgSufS-HA were grown for
682 three days in the presence of ATc. Then they were mechanically released from their host cells,
683 purified on a glass wool fiber column, washed in Hanks' Balanced Salt Solution (Gibco). Samples were
684 first normalized on parasite counts, but further adjustment was performed after parasite pellet
685 resuspension in SDS lysis buffer (50 mm Tris-HCl pH8, 10 mm EDTA pH8, 1% SDS) and protein
686 quantification with a bicinchoninic acid assay kit (Abcam). For each condition, 20 µg of total proteins
687 were separated on a 12% SDS-PAGE run for 20 min at 100 V, stained with colloidal blue (Thermo
688 Fisher Scientific), and each lane was cut in three identical fractions. Trypsin digestion and mass
689 spectrometry analysis in the Q Exactive Plus mass spectrometer (Thermo Fisher Scientific) were
690 carried out as described previously (117).

691 For peptide identification and quantification, the raw files were analyzed with MaxQuant version
692 1.6.10.43 using default settings. The minimal peptide length was set to 6. Carbamidomethylation of
693 cysteine was selected as a fixed modification and oxidation of methionine, N-terminal-
694 pyroglutamylation of glutamine and glutamate and acetylation (protein N terminus) as variable
695 modifications. Up to two missed cleavages were allowed. The files were searched against the *T.*
696 *gondii* proteome (March 2020 -https: //www.uniprot.org/proteomes/UP000005641-8450 entries).
697 Identified proteins were filtered according to the following criteria: at least two different trypsin
698 peptides with at least one unique peptide, an *E* value below 0.01 and a protein E value smaller than
699 0.01 were required. Using the above criteria, the rate of false peptide sequence assignment and false
700 protein identification were lower than 1%. Peptide ion intensity values derived from MaxQuant were
701 subjected for label-free quantitation. Unique and razor peptides were considered (118). Statistical
702 analyses were carried out using R package software. ANOVA test with threshold of 0.05 was applied
703 to identify the significant differences in the protein abundance. Hits were retained if they were
704 quantified in at least three of the four replicates in at least one experiment. Additional candidates
705 that consistently showed absence or presence of LFQ values versus the control, and mean LFQ was
706 only considered if peptides were detected in at least 3 out of the four biological replicates.

707 **Statistical analysis for phenotypic assays.** Unless specified, values are usually expressed as means ±
708 standard error of the mean (SEM). Data were analysed for comparison using unpaired Student's
709 t-test with equal variance (homoscedastic) for different samples or paired Student's t-test for similar
710 samples before and after treatment.

711 **Data availability.** All raw MS data and MaxQuant files generated have been deposited to the
712 ProteomeXchange Consortium via the PRIDE partner repository
713 (https://www.ebi.ac.uk/pride/archive) with the dataset identifier PXD023854.

714

715 **Acknowledgements**

716 We are grateful to P. Bradley, B. Striepen, L. Sheiner, V. Carruthers, S. Lourido and D. Soldati-Favre
717 for providing antibodies and plasmids. We thank the developers and the managers of the
718 VeupathDB.org/ToxoDB.org databases, as well as scientists who contributed datasets. We also thank
719 the MRI imaging facility for providing access to their microscopes and flow cytometers, and the Mass
720 Spectrometry Proteomics Platform (MSPP) of the BPMP laboratory. Thanks to Y. Bordat for helping
721 with the flow cytometry results and to F. Vignols for insights into the biochemistry of Fe-S proteins.

This project was supported by the Fondation pour la Recherche Médicale (Equipe FRM EQ20170336725), the Labex Parafrap (ANR-11-LABX-0024) and the Agence Nationale de la Recherche (ANR-19-CE15-0023).

References

1. Zimorski V, Ku C, Martin WF, Gould SB. 2014. Endosymbiotic theory for organelle origins. Current Opinion in Microbiology 22:38–48.

2. Spinelli JB, Haigis MC. 2018. The multifaceted contributions of mitochondria to cellular metabolism. Nat Cell Biol 20:745–754.

3. Rolland N, Bouchnak I, Moyet L, Salvi D, Kuntz M. 2018. The main functions of plastids, p. 73–85. *In* Maréchal, E (ed.), Plastids. Springer US, New York, NY.

4. Inaba T, Ito-Inaba Y. 2010. Versatile roles of plastids in plant growth and development. Plant and Cell Physiology 51:1847–1853.

5. Bowsher CG. 2001. Compartmentation of metabolism within mitochondria and plastids. Journal of Experimental Botany 52:513–527.

6. Raghavendra AS, Padmasree K. 2003. Beneficial interactions of mitochondrial metabolism with photosynthetic carbon assimilation. Trends in Plant Science 8:546–553.

7. McFadden GI, Reith ME, Munholland J, Lang-Unnasch N. 1996. Plastid in human parasites. Nature 381:482–482.

8. Fichera ME, Roos DS. 1997. A plastid organelle as a drug target in apicomplexan parasites. Nature 390:407–409.

9. Keeling PJ. 2013. The number, speed, and impact of plastid endosymbioses in eukaryotic evolution. Annu Rev Plant Biol 64:583–607.

747 10. Gould SB, Maier U-G, Martin WF. 2015. Protein import and the origin of red complex plastids.
748 Current Biology 25:R515–R521.

749 11. van Dooren GG, Striepen B. 2013. The algal past and parasite present of the apicoplast. Annu Rev
750 Microbiol 67:271–289.

751 12. Sheiner L, Vaidya AB, McFadden GI. 2013. The metabolic roles of the endosymbiotic organelles of
752 Toxoplasma and Plasmodium spp. Curr Opin Microbiol 16:452–458.

753 13. van Dooren GG, Hapuarachchi SV. 2017. The dark side of the chloroplast: biogenesis, metabolism
754 and membrane biology of the apicoplast, p. 145–185. *In* Advances in Botanical Research.
755 Elsevier.

756 14. de Souza W, Attias M, Rodrigues JCF. 2009. Particularities of mitochondrial structure in parasitic
757 protists (Apicomplexa and Kinetoplastida). The International Journal of Biochemistry & Cell
758 Biology 41:2069–2080.

759 15. Ovciarikova J, Lemgruber L, Stilger KL, Sullivan WJ, Sheiner L. 2017. Mitochondrial behaviour
760 throughout the lytic cycle of Toxoplasma gondii. Sci Rep 7:42746.

761 16. Seeber F, Limenitakis J, Soldati-Favre D. 2008. Apicomplexan mitochondrial metabolism: a story
762 of gains, losses and retentions. Trends in Parasitology 24:468–478.

763 17. Kobayashi T, Sato S, Takamiya S, Komaki-Yasuda K, Yano K, Hirata A, Onitsuka I, Hata M, Mi-ichi
764 F, Tanaka T, Hase T, Miyajima A, Kawazu S, Watanabe Y, Kita K. 2007. Mitochondria and
765 apicoplast of Plasmodium falciparum: Behaviour on subcellular fractionation and the implication.
766 Mitochondrion 7:125–132.

767 18. Nishi M, Hu K, Murray JM, Roos DS. 2008. Organellar dynamics during the cell cycle of
768 Toxoplasma gondii. J Cell Sci 121:1559–1568.

769 19. Dunay IR, Gajurel K, Dhakal R, Liesenfeld O, Montoya JG. 2018. Treatment of toxoplasmosis:
770 historical perspective, animal models, and current clinical practice. Clin Microbiol Reviews
771 31:e00057-17, /cmr/31/4/e00057-17.atom.

772 20. Lee Y, Choi JY, Fu H, Harvey C, Ravindran S, Roush WR, Boothroyd JC, Khosla C. 2011. Chemistry
773 and biology of macrolide antiparasitic agents. J Med Chem 54:2792–2804.

774 21. Hudson AT, Dickins M, Ginger CD, Gutteridge WE, Holdich T, Hutchinson DB, Pudney M, Randall
775 AW, Latter VS. 1991. 566C80: a potent broad spectrum anti-infective agent with activity against
776 malaria and opportunistic infections in AIDS patients. Drugs Exp Clin Res 17:427–435.

777 22. Lill R. 2009. Function and biogenesis of iron–sulphur proteins. Nature 460:831–838.

778 23. Roche B, Aussel L, Ezraty B, Mandin P, Py B, Barras F. 2013. Iron/sulfur proteins biogenesis in
779 prokaryotes: formation, regulation and diversity. Biochimica et Biophysica Acta (BBA) -
780 Bioenergetics 1827:455–469.

781 24. Zheng L, Cash VL, Flint DH, Dean DR. 1998. Assembly of Iron-Sulfur Clusters: identification of an
782 iscSUA-hscBA-fdx gene cluster from Azotobacter vinelandii. J Biol Chem 273:13264–13272.

783 25. Takahashi Y, Tokumoto U. 2002. A third bacterial system for the assembly of Iron-Sulfur clusters
784 with homologs in archaea and plastids. J Biol Chem 277:28380–28383.

785 26. Boyd ES, Thomas KM, Dai Y, Boyd JM, Outten FW. 2014. Interplay between Oxygen and Fe–S
786 cluster biogenesis: insights from the Suf pathway. Biochemistry 53:5834–5847.

787 27. Tsaousis AD. 2019. On the origin of Iron/Sulfur cluster biosynthesis in eukaryotes. Front
788 Microbiol 10:2478.

789 28. Couturier J, Touraine B, Briat J-F, Gaymard F, Rouhier N. 2013. The iron-sulfur cluster assembly
790 machineries in plants: current knowledge and open questions. Front Plant Sci 4.

791 29. Lill R, Srinivasan V, Mühlenhoff U. 2014. The role of mitochondria in cytosolic-nuclear iron–sulfur
792 protein biogenesis and in cellular iron regulation. Current Opinion in Microbiology 22:111–119.

793 30. Aw YTV, Seidi A, Hayward JA, Lee J, Victor Makota F, Rug M, van Dooren GG. 2020. A key
794 cytosolic iron-sulfur cluster synthesis protein localises to the mitochondrion of Toxoplasma
795 gondii. Mol Microbiol mmi.14651.

796 31. Gisselberg JE, Dellibovi-Ragheb TA, Matthews KA, Bosch G, Prigge ST. 2013. The Suf iron-sulfur
797 cluster synthesis pathway is required for apicoplast maintenance in malaria parasites. PLoS
798 Pathog 9:e1003655.

799 32. Haussig JM, Matuschewski K, Kooij TWA. 2014. Identification of vital and dispensable sulfur
800 utilization factors in the Plasmodium apicoplast. PLoS ONE 9:e89718.

801 33. Kumar B, Chaubey S, Shah P, Tanveer A, Charan M, Siddiqi MI, Habib S. 2011. Interaction
802 between sulphur mobilisation proteins SufB and SufC: Evidence for an iron–sulphur cluster
803 biogenesis pathway in the apicoplast of Plasmodium falciparum. International Journal for
804 Parasitology 41:991–999.

805 34. Charan M, Singh N, Kumar B, Srivastava K, Siddiqi MI, Habib S. 2014. Sulfur mobilization for Fe-S
806 cluster assembly by the essential SUF pathway in the Plasmodium falciparum apicoplast and its
807 Inhibition. Antimicrob Agents Chemother 58:3389–3398.

808 35. Charan M, Choudhary HH, Singh N, Sadik M, Siddiqi MI, Mishra S, Habib S. 2017. [Fe-S] cluster
809 assembly in the apicoplast and its indispensability in mosquito stages of the malaria parasite.
810 FEBS J 284:2629–2648.

811 36. Pala ZR, Saxena V, Saggu GS, Garg S. 2018. Recent advances in the [Fe–S] cluster biogenesis (SUF)
812 pathway functional in the apicoplast of Plasmodium. Trends in Parasitology 34:800–809.

813 37. Mazumdar J, H Wilson E, Masek K, A Hunter C, Striepen B. 2006. Apicoplast fatty acid synthesis is
814 essential for organelle biogenesis and parasite survival in Toxoplasma gondii. Proc Natl Acad Sci
815 USA 103:13192–13197.

816 38. Nair SC, Brooks CF, Goodman CD, Sturm A, Strurm A, McFadden GI, Sundriyal S, Anglin JL, Song Y,
817 Moreno SNJ, Striepen B. 2011. Apicoplast isoprenoid precursor synthesis and the molecular basis
818 of fosmidomycin resistance in Toxoplasma gondii. J Exp Med 208:1547–1559.

819 39. Bergmann A, Floyd K, Key M, Dameron C, Rees KC, Thornton LB, Whitehead DC, Hamza I, Dou Z.
820 2020. Toxoplasma gondii requires its plant-like heme biosynthesis pathway for infection. PLoS
821 Pathog 16:e1008499.

822 40. Tjhin ET, Hayward JA, McFadden GI, van Dooren GG. 2020. Characterization of the apicoplast-
823 localized enzyme TgUroD in Toxoplasma gondii reveals a key role of the apicoplast in heme
824 biosynthesis. J Biol Chem 295:1539–1550.

825 41. Harb OS, Roos DS. 2020. ToxoDB: functional genomics resource for Toxoplasma and related
826 organisms. Methods Mol Biol 2071:27–47.

827 42. Barylyuk K, Koreny L, Ke H, Butterworth S, Crook OM, Lassadi I, Gupta V, Tromer E, Mourier T,
828 Stevens TJ, Breckels LM, Pain A, Lilley KS, Waller RF. 2020. A comprehensive subcellular atlas of
829 the Toxoplasma proteome via hyperLOPIT provides spatial context for protein functions. Cell
830 Host & Microbe S193131282030514X.

831 43. Sidik SM, Huet D, Ganesan SM, Huynh M-H, Wang T, Nasamu AS, Thiru P, Saeij JPJ, Carruthers
832 VB, Niles JC, Lourido S. 2016. A Genome-wide CRISPR Screen in Toxoplasma Identifies Essential
833 Apicomplexan Genes. Cell 166:1423-1435.e12.

834 44. Fox BA, Ristuccia JG, Gigley JP, Bzik DJ. 2009. Efficient gene replacements in Toxoplasma gondii
835 strains deficient for nonhomologous end joining. Eukaryotic Cell 8:520–529.

836 45. Huynh M-H, Carruthers VB. 2009. Tagging of endogenous genes in a Toxoplasma gondii strain
837 lacking Ku80. Eukaryot Cell 8:530–539.

838 46. Sheiner L, Demerly JL, Poulsen N, Beatty WL, Lucas O, Behnke MS, White MW, Striepen B. 2011.
839 A Systematic Screen to Discover and Analyze Apicoplast Proteins Identifies a Conserved and
840 Essential Protein Import Factor. PLoS Pathog 7.

841 47. Pino P, Foth BJ, Kwok L-Y, Sheiner L, Schepers R, Soldati T, Soldati-Favre D. 2007. Dual targeting
842 of antioxidant and metabolic enzymes to the mitochondrion and the apicoplast of Toxoplasma
843 gondii. PLoS Pathog 3:e115.

844 48. Ollagnier-de-Choudens S, Lascoux D, Loiseau L, Barras F, Forest E, Fontecave M. 2003.
845 Mechanistic studies of the SufS-SufE cysteine desulfurase: evidence for sulfur transfer from SufS
846 to SufE. FEBS Lett 555:263–267.

847 49. Narayana Murthy, UM, Ollagnier-de-Choudens S, Sanakis Y, Abdel-Ghany SE, Rousset C, Ye H,
848 Fontecave M, Pilon-Smits EAH, Pilon M. 2007. Characterization of Arabidopsis thaliana SufE2 and
849 SufE3: functions in chloroplast iron-sulfur cluster assembly and NAD synthesis. J Biol Chem
850 282:18254–18264.

851 50. Meissner M, Brecht S, Bujard H, Soldati D. 2001. Modulation of myosin A expression by a newly
852 established tetracycline repressor-based inducible system in Toxoplasma gondii. Nucleic Acids
853 Res 29:E115.

854 51. Pfefferkorn ER, Nothnagel RF, Borotz SE. 1992. Parasiticidal effect of clindamycin on Toxoplasma
855 gondii grown in cultured cells and selection of a drug-resistant mutant. Antimicrob Agents
856 Chemother 36:1091–1096.

857 52. He CY, Shaw MK, Pletcher CH, Striepen B, Tilney LG, Roos DS. 2001. A plastid segregation defect
858 in the protozoan parasite Toxoplasma gondii. EMBO J 20:330–339.

859 53. Blader IJ, Coleman BI, Chen C-T, Gubbels M-J. 2015. Lytic cycle of Toxoplasma gondii: 15 years
860 later. Annu Rev Microbiol 69:463–485.

861 54. Dubey JP, Lindsay DS, Speer CA. 1998. Structures of Toxoplasma gondii tachyzoites, bradyzoites,
862 and sporozoites and biology and development of tissue cysts. Clin Microbiol Rev 11:267–299.

863 55. Cerutti A, Blanchard N, Besteiro S. 2020. The bradyzoite: a key developmental stage for the
864 persistence and pathogenesis of toxoplasmosis. Pathogens 9.

865 56. Valasatava Y, Rosato A, Banci L, Andreini C. 2016. MetalPredator: a web server to predict iron-
866 sulfur cluster binding proteomes. Bioinformatics 32:2850–2852.

867 57. Fuss JO, Tsai C-L, Ishida JP, Tainer JA. 2015. Emerging critical roles of Fe–S clusters in DNA
868 replication and repair. Biochimica et Biophysica Acta (BBA) - Molecular Cell Research 1853:1253–
869 1271.

870 58. Thomsen-Zieger N, Schachtner J, Seeber F. 2003. Apicomplexan parasites contain a single lipoic
871 acid synthase located in the plastid. FEBS Lett 547:80–86.

872 59. Pierrel F, Douki T, Fontecave M, Atta M. 2004. MiaB protein is a bifunctional radical-S-
873 adenosylmethionine enzyme involved in thiolation and methylation of tRNA. J Biol Chem
874 279:47555–47563.

875 60. Imlay L, Odom AR. 2014. Isoprenoid metabolism in apicomplexan parasites. Curr Clin Microbiol
876 Rep 1:37–50.

877 61. Seidi A, Muellner-Wong LS, Rajendran E, Tjhin ET, Dagley LF, Aw VY, Faou P, Webb AI, Tonkin CJ,
878 van Dooren GG. 2018. Elucidating the mitochondrial proteome of Toxoplasma gondii reveals the
879 presence of a divergent cytochrome c oxidase. Elife 7.

880 62. Hayward JA, Rajendran E, Zwahlen SM, Faou P, van Dooren GG. 2020. Divergent features of the
881 coenzyme Q:cytochrome c oxidoreductase complex in Toxoplasma gondii parasites. preprint,
882 Microbiology.

883 63. Maclean AE, Bridges HR, Silva MF, Ding S, Hirst J, Sheiner L. 2020. Complexome profile of
884 Toxoplasma gondii mitochondria identifies a divergent cytochrome bc1 complex. preprint, Cell
885 Biology.

886 64. Lanz ND, Booker SJ. 2015. Auxiliary iron–sulfur cofactors in radical SAM enzymes. Biochimica et
887 Biophysica Acta (BBA) - Molecular Cell Research 1853:1316–1334.

888 65. Pittman KJ, Aliota MT, Knoll LJ. 2014. Dual transcriptional profiling of mice and Toxoplasma
889 gondii during acute and chronic infection. BMC Genomics 15:806.

890 66. Hehl AB, Basso WU, Lippuner C, Ramakrishnan C, Okoniewski M, Walker RA, Grigg ME, Smith NC,
891 Deplazes P. 2015. Asexual expansion of Toxoplasma gondii merozoites is distinct from
892 tachyzoites and entails expression of non-overlapping gene families to attach, invade, and
893 replicate within feline enterocytes. BMC Genomics 16:66.

894 67. Jung C, Lee CY-F, Grigg ME. 2004. The SRS superfamily of Toxoplasma surface proteins.
895 International Journal for Parasitology 34:285–296.

896 68. Li L, Brunk BP, Kissinger JC, Pape D, Tang K, Cole RH, Martin J, Wylie T, Dante M, Fogarty SJ, Howe
897 DK, Liberator P, Diaz C, Anderson J, White M, Jerome ME, Johnson EA, Radke JA, Stoeckert CJ,
898 Waterston RH, Clifton SW, Roos DS, Sibley LD. 2003. Gene discovery in the apicomplexa as
899 revealed by EST sequencing and assembly of a comparative gene database. Genome Res 13:443–
900 454.

901 69. Tomita T, Bzik DJ, Ma YF, Fox BA, Markillie LM, Taylor RC, Kim K, Weiss LM. 2013. The
902 Toxoplasma gondii cyst wall protein CST1 is critical for cyst wall integrity and promotes
903 bradyzoite persistence. PLoS Pathog 9:e1003823.

904 70. Yang J, Zhang L, Diao H, Xia N, Zhou Y, Zhao J, Shen B. 2017. ANK1 and DnaK-TPR, two
905 tetratricopeptide repeat-containing proteins primarily expressed in Toxoplasma bradyzoites, do
906 not contribute to bradyzoite differentiation. Front Microbiol 8:2210.

907 71. Nadipuram SM, Thind AC, Rayatpisheh S, Wohlschlegel JA, Bradley PJ. 2020. Proximity
908 biotinylation reveals novel secreted dense granule proteins of Toxoplasma gondii bradyzoites.
909 PLoS One 15:e0232552.

910 72. Kawamukai M. 2016. Biosynthesis of coenzyme Q in eukaryotes. Bioscience, Biotechnology, and
911 Biochemistry 80:23–33.

912 73. Ramakrishnan S, Docampo MD, Macrae JI, Pujol FM, Brooks CF, van Dooren GG, Hiltunen JK,
913 Kastaniotis AJ, McConville MJ, Striepen B. 2012. Apicoplast and endoplasmic reticulum
914 cooperate in fatty acid biosynthesis in apicomplexan parasite Toxoplasma gondii. J Biol Chem
915 287:4957–4971.

916 74. Amiar S, MacRae JI, Callahan DL, Dubois D, van Dooren GG, Shears MJ, Cesbron-Delauw M-F,
917 Maréchal E, McConville MJ, McFadden GI, Yamaryo-Botté Y, Botté CY. 2016. Apicoplast-localized
918 lysophosphatidic acid precursor assembly is required for bulk phospholipid synthesis in
919 Toxoplasma gondii and relies on an algal/plant-like glycerol 3-phosphate acyltransferase. PLOS
920 Pathogens 12:e1005765.

921 75. Dubois D, Fernandes S, Amiar S, Dass S, Katris NJ, Botté CY, Yamaryo-Botté Y. 2018. Toxoplasma
922 gondii acetyl-CoA synthetase is involved in fatty acid elongation (of long fatty acid chains) during
923 tachyzoite life stages. J Lipid Res 59:994–1004.

924 76. Bohne W, Heesemann J, Gross U. 1994. Reduced replication of Toxoplasma gondii is necessary
925 for induction of bradyzoite-specific antigens: a possible role for nitric oxide in triggering stage
926 conversion. Infect Immun 62:1761–1767.

927 77. Crack JC, Green J, Thomson AJ, Le Brun NE. 2014. Iron-sulfur clusters as biological sensors: the
928 chemistry of reactions with molecular oxygen and nitric oxide. Acc Chem Res 47:3196–3205.

929 78. Soete M, Fortier B, Camus D, Dubremetz JF. 1993. Toxoplasma gondii: kinetics of bradyzoite-
930 tachyzoite interconversion in vitro. Exp Parasitol 76:259–264.

931 79. Biddau M, Sheiner L. 2019. Targeting the apicoplast in malaria. Biochem Soc Trans 47:973–983.

932 80. Mather MW, Henry KW, Vaidya AB. 2007. Mitochondrial drug targets in apicomplexan parasites.
933 Curr Drug Targets 8:49–60.

934 81. Goodman CD, Pasaje CFA, Kennedy K, McFadden GI, Ralph SA. 2016. Targeting protein
935 translation in organelles of the Apicomplexa. Trends in Parasitology 32:953–965.

936 82. Baggish AL, Hill DR. 2002. Antiparasitic agent atovaquone. Antimicrob Agents Chemother
937 46:1163–1173.

938 83. Tomavo S, Boothroyd JC. 1995. Interconnection between organellar functions, development and
939 drug resistance in the protozoan parasite, Toxoplasma gondii. International Journal for
940 Parasitology 25:1293–1299.

941 84. Gross U, Pohl F. 1996. Influence of antimicrobial agents on replication and stage conversion of
942 Toxoplasma gondii. Curr Top Microbiol Immunol 219:235–245.

943 85. Kennedy K, Crisafulli EM, Ralph SA. 2019. Delayed death by plastid inhibition in apicomplexan
944 parasites. Trends in Parasitology 35:747–759.

945 86. Liang X, Cui J, Yang X, Xia N, Li Y, Zhao J, Gupta N, Shen B. 2020. Acquisition of exogenous fatty
946 acids renders apicoplast-based biosynthesis dispensable in tachyzoites of Toxoplasma. J Biol
947 Chem 295:7743–7752.

948 87. Amiar S, Katris NJ, Berry L, Dass S, Duley S, Arnold C-S, Shears MJ, Brunet C, Touquet B,
949 McFadden GI, Yamaryo-Botté Y, Botté CY. 2020. Division and adaptation to host environment of
950 apicomplexan parasites depend on apicoplast lipid metabolic plasticity and host organelle
951 remodeling. Cell Reports 30:3778-3792.e9.

952 88. MacRae JI, Sheiner L, Nahid A, Tonkin C, Striepen B, McConville MJ. 2012. Mitochondrial
953 metabolism of glucose and glutamine is required for intracellular growth of Toxoplasma gondii.
954 Cell Host Microbe 12:682–692.

955 89. Shukla A, Olszewski KL, Llinás M, Rommereim LM, Fox BA, Bzik DJ, Xia D, Wastling J, Beiting D,
956 Roos DS, Shanmugam D. 2018. Glycolysis is important for optimal asexual growth and formation
957 of mature tissue cysts by Toxoplasma gondii. International Journal for Parasitology 48:955–968.

958 90. Denton H, Roberts CW, Alexander J, Thong KW, Coombs GH. 1996. Enzymes of energy
959 metabolism in the bradyzoites and tachyzoites of Toxoplasma gondii. FEMS Microbiol Lett
960 137:103–108.

961 91. Dzierszinski F, Nishi M, Ouko L, Roos DS. 2004. Dynamics of Toxoplasma gondii differentiation.
962 Eukaryotic Cell 3:992–1003.

963 92. Watts E, Zhao Y, Dhara A, Eller B, Patwardhan A, Sinai AP. 2015. Novel Approaches Reveal that
964 Toxoplasma gondii Bradyzoites within Tissue Cysts Are Dynamic and Replicating Entities In Vivo.
965 MBio 6:e01155-01115.

966 93. Sibley LD, Boothroyd JC. 1992. Virulent strains of Toxoplasma gondii comprise a single clonal
967 lineage. Nature 359:82–85.

968 94. McHugh TD, Holliman RE, Butcher PD. 1994. The in vitro model of tissue cyst formation in
969 Toxoplasma gondii. Parasitology Today 10:281–285.

970 95. Chandel NS. 2015. Evolution of mitochondria as signaling organelles. Cell Metab 22:204–206.

971 96. Martínez-Reyes I, Diebold LP, Kong H, Schieber M, Huang H, Hensley CT, Mehta MM, Wang T,
972 Santos JH, Woychik R, Dufour E, Spelbrink JN, Weinberg SE, Zhao Y, DeBerardinis RJ, Chandel NS.
973 2016. TCA cycle and mitochondrial membrane potential are necessary for diverse biological
974 functions. Mol Cell 61:199–209.

975 97. Sagot I, Laporte D. 2019. The cell biology of quiescent yeast – a diversity of individual scenarios. J
976 Cell Sci 132:jcs213025.

977 98. Waldman BS, Schwarz D, Wadsworth MH, Saeij JP, Shalek AK, Lourido S. 2020. Identification of a
978 master regulator of differentiation in Toxoplasma. Cell S0092867419313753.

979 99. Hassan MA, Vasquez JJ, Guo-Liang C, Meissner M, Nicolai Siegel T. 2017. Comparative ribosome
980 profiling uncovers a dominant role for translational control in Toxoplasma gondii. BMC Genomics
981 18:961.

982 100. Holmes MJ, Augusto L da S, Zhang M, Wek RC, Sullivan WJ. 2017. Translational control in the
983 latency of apicomplexan parasites. Trends in Parasitology 33:947–960.

984 101. Harvey R, Dezi V, Pizzinga M, Willis AE. 2017. Post-transcriptional control of gene expression
985 following stress: the role of RNA-binding proteins. Biochem Soc Trans 45:1007–1014.

986 102. Lirussi D, Matrajt M. 2011. RNA granules present only in extracellular Toxoplasma gondii
987 increase parasite viability. Int J Biol Sci 7:960–967.

988 103. Liu M, Miao J, Liu T, Sullivan WJ, Cui L, Chen X. 2014. Characterization of TgPuf1, a member of
989 the Puf family RNA-binding proteins from Toxoplasma gondii. Parasit Vectors 7:141.

990 104. Gissot M, Walker R, Delhaye S, Alayi TD, Huot L, Hot D, Callebaut I, Schaeffer-Reiss C,
991 Dorsselaer AV, Tomavo S. 2013. Toxoplasma gondii Alba proteins are involved in translational
992 control of gene expression. J Mol Biol 425:1287–1301.

993 105. Gastens MH, Fischer H-G. 2002. Toxoplasma gondii eukaryotic translation initiation factor 4A
994 associated with tachyzoite virulence is down-regulated in the bradyzoite stage. Int J Parasitol
995 32:1225–1234.

996 106. Balk J, Pilon M. 2011. Ancient and essential: the assembly of iron–sulfur clusters in plants.
997 Trends in Plant Science 16:218–226.

998 107. Shanmugasundram A, Gonzalez-Galarza FF, Wastling JM, Vasieva O, Jones AR. 2013. Library
999 of Apicomplexan Metabolic Pathways: a manually curated database for metabolic pathways of
1000 apicomplexan parasites. Nucleic Acids Research 41:D706–D713.

1001 108. Outten FW, Djaman O, Storz G. 2004. A suf operon requirement for Fe-S cluster assembly
1002 during iron starvation in Escherichia coli: suf operon role during iron starvation. Molecular
1003 Microbiology 52:861–872.

1004 109. Morlon-Guyot J, Berry L, Chen C-T, Gubbels M-J, Lebrun M, Daher W. 2014. The Toxoplasma
1005 gondii calcium-dependent protein kinase 7 is involved in early steps of parasite division and is
1006 crucial for parasite survival. Cell Microbiol 16:95–114.

1007 110. Couvreur G, Sadak A, Fortier B, Dubremetz JF. 1988. Surface antigens of Toxoplasma gondii.
1008 Parasitology 97 (Pt 1):1–10.

1009 111. Agrawal S, van Dooren GG, Beatty WL, Striepen B. 2009. Genetic evidence that an
1010 endosymbiont-derived endoplasmic reticulum-associated protein degradation (ERAD) system
1011 functions in import of apicoplast proteins. J Biol Chem 284:33683–33691.

1012 112. Herm-Gotz A. 2002. Toxoplasma gondii myosin A and its light chain: a fast, single-headed,
1013 plus-end-directed motor. The EMBO Journal 21:2149–2158.

1014 113. Bermudes D, Dubremetz J-F, Achbarou A, Joiner KA. 1994. Cloning of a cDNA encoding the
1015 dense granule protein GRA3 from Toxoplasma gondii. Molecular and Biochemical Parasitology
1016 68:247–257.

1017 114. Plattner F, Yarovinsky F, Romero S, Didry D, Carlier M-F, Sher A, Soldati-Favre D. 2008.
1018 Toxoplasma profilin is essential for host cell invasion and TLR11-dependent induction of an
1019 interleukin-12 response. Cell Host Microbe 3:77–87.

1020 115. Tomavo S, Fortier B, Soete M, Ansel C, Camus D, Dubremetz JF. 1991. Characterization of
1021 bradyzoite-specific antigens of Toxoplasma gondii. Infect Immun 59:3750–3753.

1022 116. Jia Y, Marq J-B, Bisio H, Jacot D, Mueller C, Yu L, Choudhary J, Brochet M, Soldati-Favre D.
1023 2017. Crosstalk between PKA and PKG controls pH-dependent host cell egress of Toxoplasma
1024 gondii. EMBO J 36:3250–3267.

1025 117. Berger N, Vignols F, Przybyla-Toscano J, Roland M, Rofidal V, Touraine B, Zienkiewicz K,
1026 Couturier J, Feussner I, Santoni V, Rouhier N, Gaymard F, Dubos C. 2020. Identification of client
1027 iron–sulfur proteins of the chloroplastic NFU2 transfer protein in Arabidopsis thaliana. Journal of
1028 Experimental Botany 71:4171–4187.

1029 118. Cox J, Mann M. 2008. MaxQuant enables high peptide identification rates, individualized
1030 p.p.b.-range mass accuracies and proteome-wide protein quantification. Nat Biotechnol
1031 26:1367–1372.

1032 **Figure legends**
1033
1034 **Figure 1. TgSufS and TgIscU are functional homologs of components of the plastidic and**
1035 **mitochondrial iron sulfur cluster synthesis pathways.**

1036 A) Putative Fe-S cluster synthesis pathways and associated molecular machinery in *Toxoplasma*. B)
1037 Functional complementation of bacterial mutants for IscU (top) and SufS (bottom). Growth of
1038 bacterial mutant strains and strains complemented ('comp') by their respective *T. gondii* homologues
1039 ('comp'), was assessed by monitoring the optical density at 600 nm in the presence or not of an iron
1040 chelator (2,2'-bipyridyl, 'chel'). Values are mean from n=3 independent experiments ±SEM. * denotes
1041 $p \leq 0.05$, Student's *t*-test.
1042
1043
1044 **Figure 2. TgSufS and TgIscU localize to the apicoplast and the mitochondrion, respectively.**
1045 Detection by immunoblot of C-terminally HA-tagged TgSufS (A) and TgIscU (B) in parasite extracts
1046 reveals the presence of both precusor (p) and mature (m) forms of the proteins. Anti-actin (TgACT1)
1047 antibody was used as a loading control. Immunofluorescence assay shows TgSufS co-localizes with
1048 apicoplast marker TgCPN60 (C) and TgIscU co-localizes with mitochondrial marker F1 β ATPase (D).
1049 Scale bar represents 5 µm. DNA was labelled with DAPI. DIC: differential interference contrast.
1050
1051
1052 **Figure 3. Efficient down-regulation of TgSufS and TgIscU expression with anhydrotetracyclin (ATc).**
1053 A) Immunoblot analysis with anti-HA antibody shows efficient down-regulation of TgSufS after 48h of
1054 incubation with ATc. Anti-SAG1 antibody was used as a loading control. B) Immunoblot analysis with
1055 anti-HA antibody shows efficient down-regulation of TgIscU after 24h of incubation with ATc. Anti-
1056 SAG1 antibody was used as a loading control. C) and D) Immunofluorescence assays show TgSufS and
1057 TgIscU are not detectable anymore after 48h of incubation with ATc. Scale bar represents 5 µm. DNA
1058 was labelled with DAPI. DIC: differential interference contrast.
1059
1060 **Figure 4. Depletion of TgSufS and TgIscU affects in vitro growth of the tachyzoites.** Plaque assays
1061 were carried out by infecting HFF monolayers with the TATi ΔKu80 cell line, the cKD TgSufS-HA (A) or
1062 the cKD TgIscU-HA (B) cell lines, or parasites complemented with a wild-type version of the
1063 respective proteins. They were grown for 7 days ± ATc. Measurements of lysis plaque areas are
1064 shown on the right and highlight a significant defect in the lytic cycle when TgSufS (A) or TgIscU (B)
1065 were depleted. Values are means of n=3 experiments ± SEM. ** denotes $p \leq 0.01$, Student's *t*-test.
1066 Scale bars= 1mm. TgSufS (C) and TgIscU (D) mutant and complemented cell lines, as well as their
1067 parental cell lines and the TATi ΔKu80 control, were grown in HFF in the presence or absence of ATc
1068 for 48 hours, and subsequently allowed to invade and grow in new HFF cells for an extra 24 hours in
1069 the presence of ATc. Parasites per vacuole were then counted. Values are means ± SEM from n=3
1070 independent experiments for which 200 vacuoles were counted for each condition. E) Plaque assays
1071 for the TgSufS and TgIscU mutants were performed as described in A) and B), but ATc was washed
1072 out after 7 days and parasites were left to grow for an extra 4 days. Plaque number and area were
1073 measured. Data are means ± SEM from three independent experiments. * $p \leq 0.05$, ** $p \leq 0.01$,
1074 Student's *t*-test. Arrowheads show plaques forming in the TgIscU upon ATc removal. Scale bar= 1mm.
1075
1076
1077 **Figure 5. Impact of TgSufS and TgIscU depletion on intracellular tachyzoites.**
1078 A) Depletion of TgSufS impacts the apicoplast. cKD TgSufS-HA parasites were kept in the presence of
1079 ATc and the aspect of the apicoplast and mitochondrion was evaluated by microscopic observation
1080 using specific markers (CPN60 and F1β ATPase, respectively). After 72 hours, parasites egressed and
1081 were used to reinvade new host cells for subsequent timepoints. Scale bar represents 5 µm. DNA was
1082 labelled with DAPI. DIC: differential interference contrast. B) Quantification of apicoplast loss in
1083 vacuoles containing cKD TgSufS-HA parasites after 72 to 120 hours of incubation with ATc. Data are
1084 mean values from n=3 independent experiments ±SEM. ** $p \leq 0.005$, **** $p \leq 0.0001$, Student's
1085 *t*-test. C) Depletion of TgIscU does not impact mitochondrial and overall parasite morphologies, but
1086 affects parasite growth. cKD TgIscU-HA parasites were grown in the presence of ATc for up to five
1087 days and the aspect of the apicoplast and mitochondrion was evaluated by microscopic observation

using specific markers described in A). Growth in the presence of ATc was continuous for up to five days. Scale bar represents 5 µm. DNA was labelled with DAPI. DIC: differential interference contrast. D) Egress is not affected by TgIscU depletion. An egress assay was performed using calcium ionophore A23187. On the left are representative images of vacuoles containing parasites that egressed normally or did not. GRA3 (parasitophorous vacuole marker) staining is shown in green and GAP45 (parasite periphery marker) in red. Scale bars= 10µm. On the right is the quantification of egress for cKD TgIscU-HA parasites kept in the presence of ATc or not. Mean values ± SEM from *n*=3 independent biological experiments are represented.

Figure 6. Change in protein expression induced by TgSufS and TgIscU depletion. A) Volcano plots showing the protein expression difference based on label-free quantitative proteomic data from TgSufS ans TgIscU mutants grown in the presence of ATc. X-axis shows log2 fold change versus the TATi ΔKu80 control grown in the same conditions, and the Y-axis shows -log10(p value) after ANOVA statistical test for *n*=4 independent biological replicates. Less abundant or more abundant proteins that were selected for analysis are displayed in red and blue, respectively. B) Venn diagram representation of the shared and unique proteins whose expression is affected by the depletion of TgSufS and TgIscU.

Figure 7. Depletion of TgSufS impacts know apicoplast Fe-S protein function, but also seem to trigger compensatory response from other cellular pathways. Classification of variant proteins according to their putative cellular localization (A) and function (B). N/A: not available; ER: endoplasmic reticulum; PM: plasma membrane; VAC: vacuolar compartment; GRA: dense granule protein; SRS: SAG-related sequence. In particular, the increased expression of ER-located lipid metabolism enzymes suggests possible compensation for loss of apicoplast-related lipid synthesis function. C) A decrease in the lipoylation of the E2 subunit of proline dehydrogenase (TgPDH-E2), which depends on the Fe-S protein LipA lipoyl synthase in the apicoplast, was observed by immunoblot using an anti-lipoic acid antibody on cell extracts from cKD TgSufS-HA parasites kept with ATc for an increasing period of time. TgCPN60 was used as a control for apicoplast integrity. TgSAG1 was used as a loading control.

Figure 8. TgIscU-depleted parasites show a marked decrease in proteins related to mitochondrial respiration, and a strong increase in bradyzoite-specific dense granules proteins and surface antigens. Classification of variant proteins according to their putative cellular localization (A) and function (B). N/A: not available; ER: endoplasmic reticulum; PM: plasma membrane; VAC: vacuolar compartment; GRA: dense granule protein; SRS: SAG-related sequence. A large proportion of components of complexes II, III and IV of the mitochondrial respiratory chain, which involve Fe-S proteins, were found to be less abundant. Conversely, the abundance of many bradyzoite-specific dense granule proteins of plasma membrane-located surface antigens increased.

Figure 9. Depletion of TgIscU stongly impacts the parasite mitochondrial membrane potential. A) TATi ΔKu80 or cKD TgIscU-HA parasites were grown in the presence of ATc, mechanically released from their host cells and labelled with the JC-1 dye. This dye exhibits potential-dependent accumulation in the mitochondrion, indicated by a switch from green fluorescence for the monomeric form of the probe, to a concentration-dependent formation of red aggregates (top left, DNA is labelled with DAPI and shown in blue, scale=1µm). B) TATi ΔKu80 (top series) or cKD TgIscU-HA parasites (bottom series) were then analysed by flow cytometry. Unlabelled parasites (no JC-1) was used as a control for gating. One representative experiment out of *n*=3 biological replicates is shown.

Figure 10. Depletion of TgIscU triggers parasite differentiation.

1139 A) cKD TgIscU-HA parasites were grown in the presence of ATc and labelled with ant-TgIMC3 (to
1140 outline parasites and spot dividing parasites) and a lectin of *Dolicos biflorus* (DBL) to specifically
1141 outline cyst walls. Scale bar represents 10 µm. DNA was labelled with DAPI. DIC: differential
1142 interference contrast. B) Quantification of DBL-positive vacuoles after 24 hours or 48 hours of culture
1143 of 1) the cKD TgIscU-HA mutant in the presence of ATc 2) the TATi ΔKu80 cell line, as a negative
1144 control, 3) the TATi ΔKu80 cell line in the presence of 100µM nitric oxide (NO), as a positive control.
1145 Data are from n=3 independent experiments. Values are mean ±SEM. * denotes $p \leq 0.05$, Student's
1146 t-test C) Clustering of bradyzoite (Bz) or tachyzoite (Tz)-specific proteins of the SRS family shows
1147 specific enrichment of bradyzoite proteins upon TgIscU depletion. D) The cKD TgIscU-HA mutant was
1148 grown for up to 20 days in the presence of ATc and labelled for tachyzoite marker SAG1), or early
1149 (P18/SAG4) or late (P21) bradyzoite markers. Scale bar represents 10 µm. DNA was labelled with
1150 DAPI. DIC: differential interference contrast. E) Measurement of the cyst area size after growing the
1151 cKD TgIscU-HA mutant for 7 and 20 days in the presence of ATc and labelling the cyst wall with DBL
1152 and measuring the surface of 60 cysts per condition. Mean ±SD is represented. One representative
1153 experiment out of n=3 independent biological replicates is shown. **** denotes $p \leq 0.0001$,
1154 Student's t-test.
1155
1156
1157 **Supplemental table legends**
1158
1159 **Table S1. Predicted Toxoplasma homologues of the iron sulfur cluster synthesis machinery.**
1160 Homology searches were conducted in ToxoBD.org using *Arabidopsis thaliana* proteins as a query.
1161 Putative subcellular localization was obtained from the hyperLOPIT data available on ToxoDB.org, or
1162 by manual annotation. CRISPR fitness score data was obtained from ToxoDB.org.
1163
1164 **Table S2. Predicted Toxoplasma iron sulfur proteome.** The Toxoplasma predicted whole proteome
1165 was obtained from the ToxoDB.org database and searched for putative iron sulfur-containing
1166 proteins with the MetalPredator web server (http://metalweb.cerm.unifi.it/tools/metalpredator/).
1167 Putative subcellular localization was obtained from the hyperLOPIT data available on ToxoDB.org, or
1168 by manual annotation. CRISPR fitness score data was obtained from ToxoDB.org.
1169
1170 **Table S3. Proteins with lower or higher expression upon depletion of TgSufS as found by label-free**
1171 **quantitative proteomics.** For each protein candidate (with www.ToxoDB.org and www.Uniprot.org
1172 identifier), $\log_2$ of the different ratio were calculated between the mean MaxQuant LFQ values
1173 ('moyLFQ') found for the IscU ('Mito') and SufS ('Apicoplast') mutants, and the TATi ΔKu80 control
1174 ('CTRL'). $-\log_{10}$(pvalue) is also provided. Putative subcellular localization was obtained from the
1175 hyperLOPIT data available on ToxoDB.org, or by manual annotation. CRISPR fitness score and
1176 transcriptomic data for tachyzoites (Tz) and bradyzoites (Bz) were obtained from ToxoDB.org.
1177
1178 **Table S4. Proteins with lower or higher expression upon depletion of TgIscU as found by label-free**
1179 **quantitative proteomics**. See legend of Table S3. Candidates from the Fe-S proteome (Table S2) that
1180 were found to have a lower expression upon TgIscU depletion are highlighted in red.
1181
1182 **Table S5. Common proteins with lower or higher expression upon depletion of TgSufS or TgIscU, as**
1183 **found by label-free quantitative proteomics.** See legend of Table S3.
1184
1185 **Table S6. Oligonucleotides used in this study.**
1186

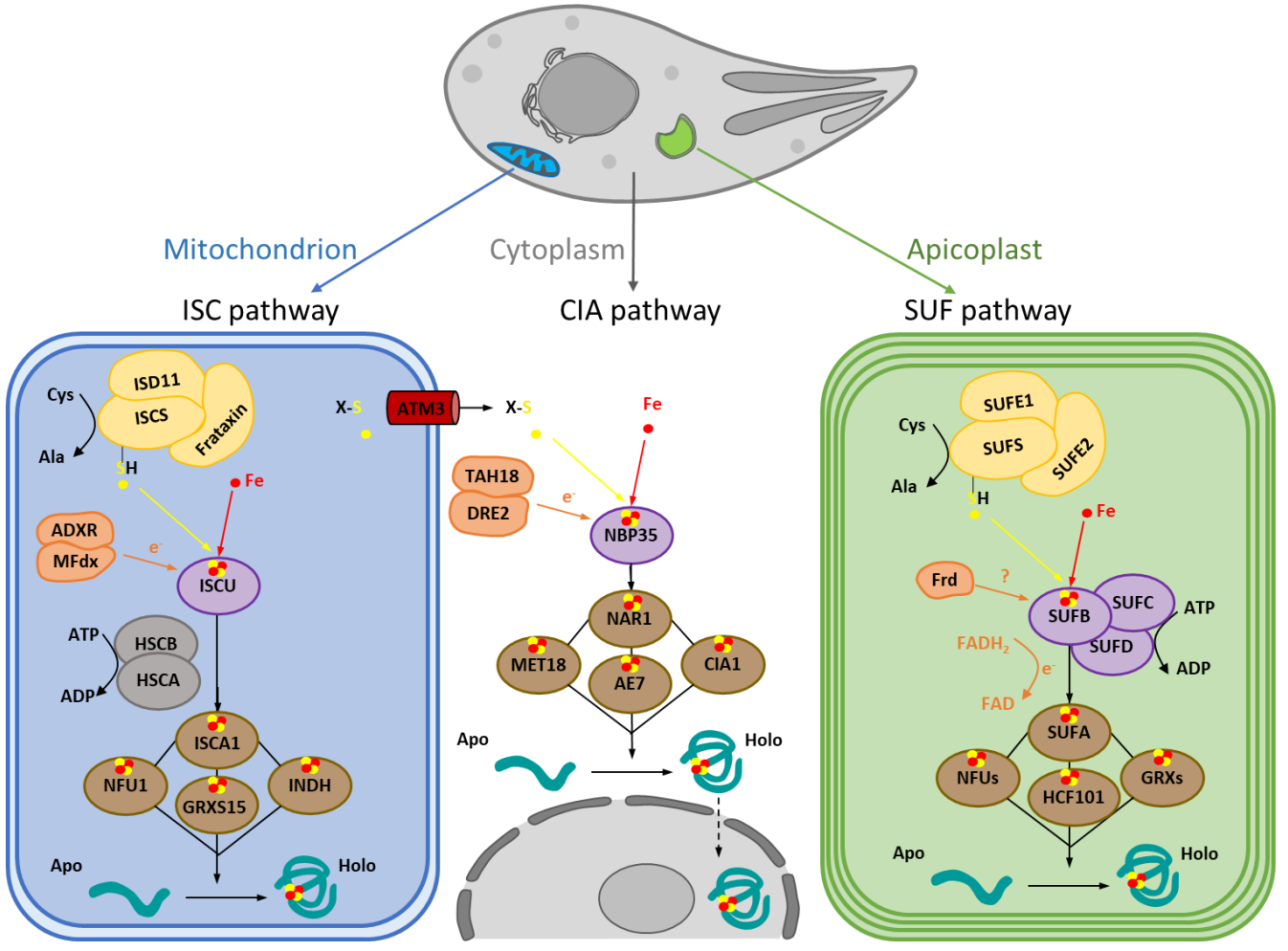
A
Mitochondrion
Cytoplasm
Apicoplast
ISC pathway
CIA pathway
SUF pathway
Cys
Ala
ISD11
ISCS
Frataxin
X-S
ATM3
Fe
ADXR
MFdx
ISCU
ATP
ADP
HSCB
HSCA
ISCA1
NFU1
GRXS15
INDH
Apo
Holo
TAH18
DRE2
NBP35
NAR1
MET18
AE7
CIA1
SUFE1
SUFS
SUFE2
Frd
SUFB
SUFC
SUFD
FADH2
FAD
SUFA
NFUs
HCF101
GRXs

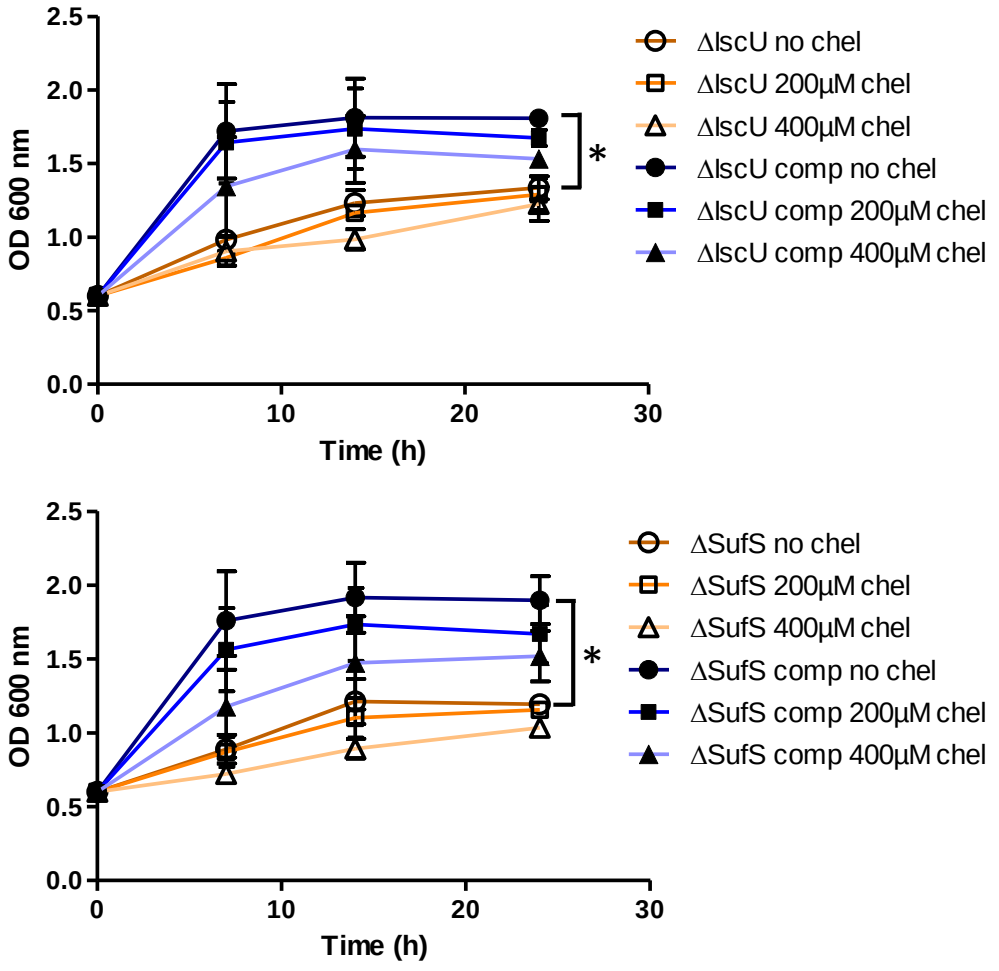
B
OD 600 nm
Time (h)
ΔIscU no chel
ΔIscU 200µM chel
ΔIscU 400µM chel
ΔIscU comp no chel
ΔIscU comp 200µM chel
ΔIscU comp 400µM chel
ΔSufS no chel
ΔSufS 200µM chel
ΔSufS 400µM chel
ΔSufS comp no chel
ΔSufS comp 200µM chel
ΔSufS comp 400µM chel
*

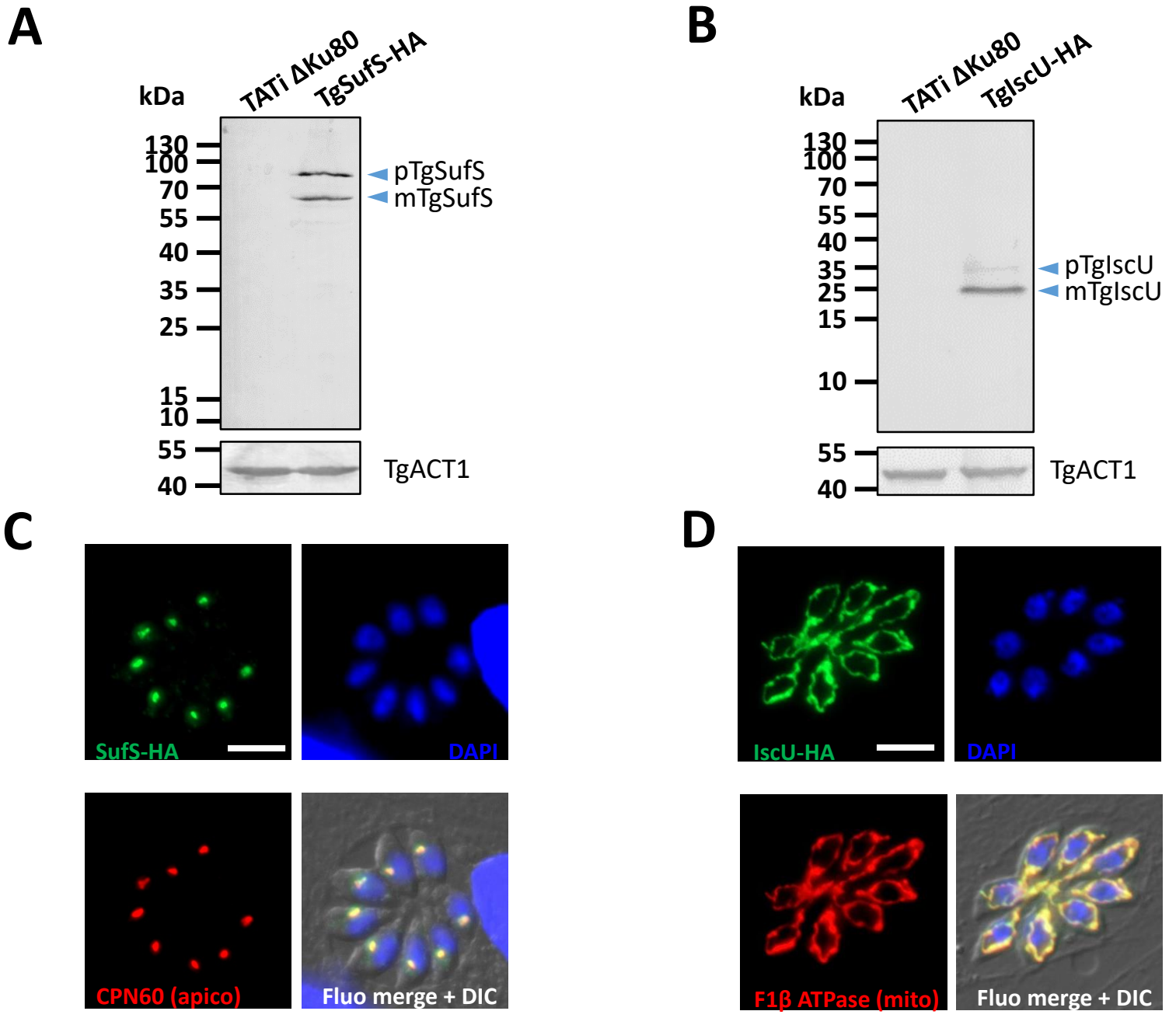
A
kDa
TATi ΔKu80
TgSufS-HA
130
100
70
55
40
35
25
15
10
pTgSufS
mTgSufS
55
40
TgACT1
B
kDa
TATi ΔKu80
TgIscU-HA
130
100
70
55
40
35
25
15
10
pTgIscU
mTgIscU
55
40
TgACT1
C
SufS-HA
DAPI
CPN60 (apico)
Fluo merge + DIC
D
IscU-HA
DAPI
F1β ATPase (mito)
Fluo merge + DIC

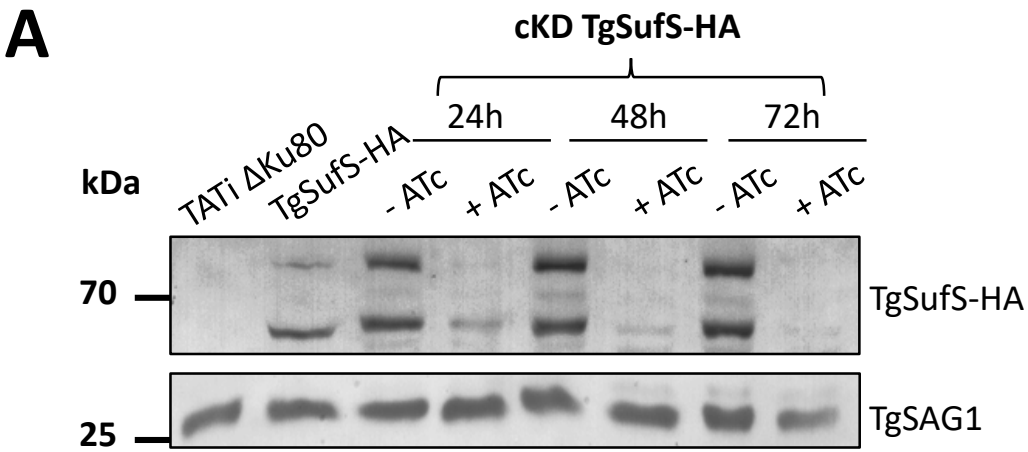
A
cKD TgSufS-HA
24h
48h
72h
kDa
TATi ΔKu80
TgSufS-HA
- ATc
+ ATc
- ATc
+ ATc
- ATc
+ ATc
70
25
TgSufS-HA
TgSAG1

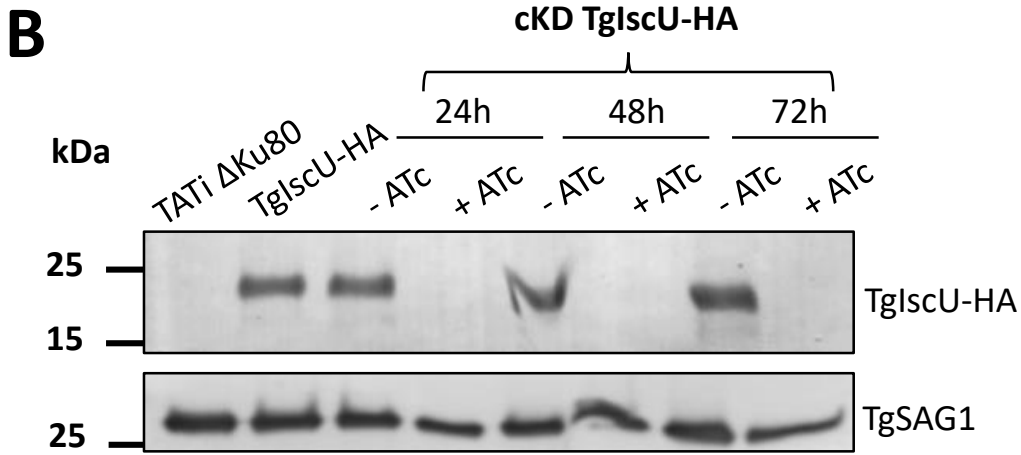
B
cKD TgIscU-HA
24h
48h
72h
kDa
TATi ΔKu80
TgIscU-HA
- ATc
+ ATc
- ATc
+ ATc
- ATc
+ ATc
25
15
25
TgIscU-HA
TgSAG1

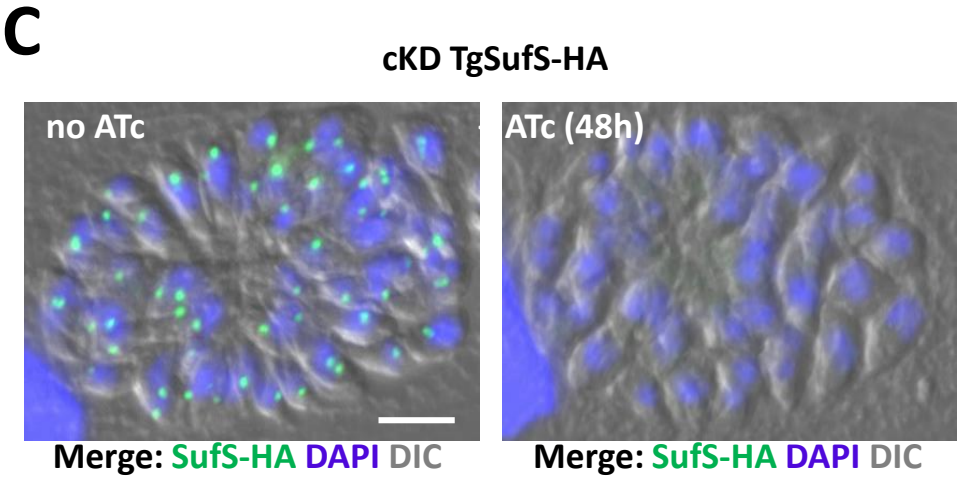
C
cKD TgSufS-HA
no ATc
ATc (48h)
Merge: SufS-HA DAPI DIC
Merge: SufS-HA DAPI DIC

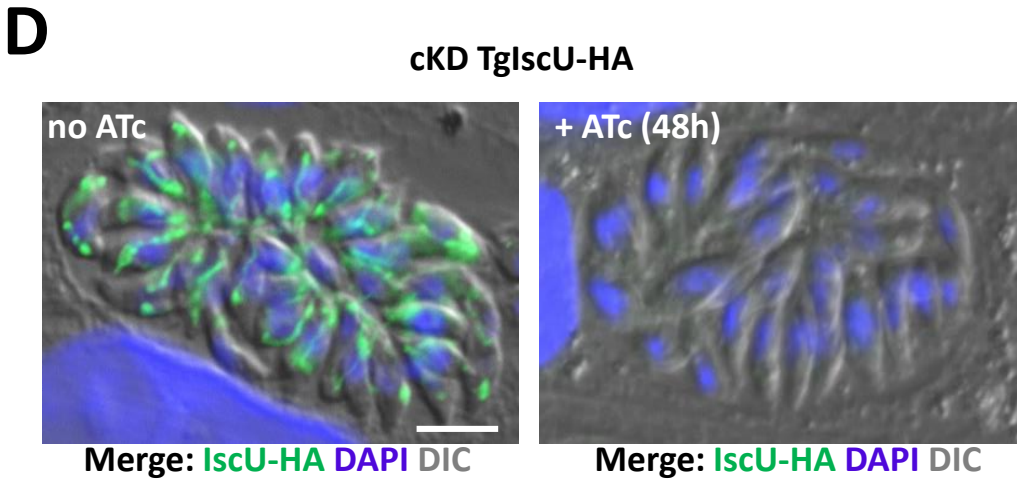
D
cKD TgIscU-HA
no ATc
+ ATc (48h)
Merge: IscU-HA DAPI DIC
Merge: IscU-HA DAPI DIC

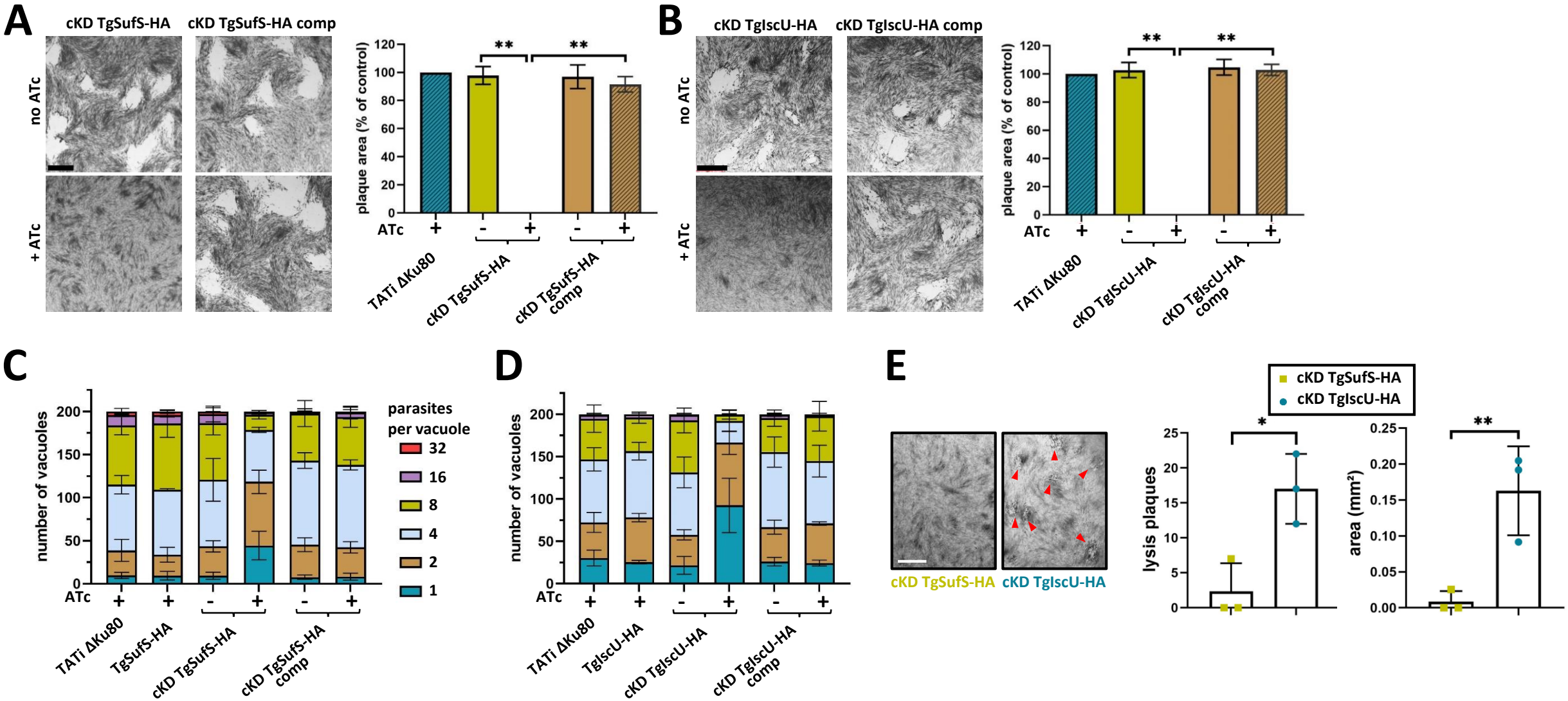
A
cKD TgSufS-HA
cKD TgSufS-HA comp
no ATc
+ ATc
plaque area (% of control)
120
100
80
60
40
20
0
**
**
ATc
+
-
+
-
+
TATi ΔKu80
cKD TgSufS-HA
cKD TgSufS-HA comp
B
cKD TgIscU-HA
cKD TgIscU-HA comp
no ATc
+ ATc
plaque area (% of control)
**
**
ATc
+
-
+
-
+
TATi ΔKu80
cKD TgIscU-HA
cKD TgIscU-HA comp
C
number of vacuoles
200
150
100
50
0
parasites per vacuole
32
16
8
4
2
1
ATc
+
+
-
+
-
+
TATi ΔKu80
TgSufS-HA
cKD TgSufS-HA
cKD TgSufS-HA comp
D
number of vacuoles
200
150
100
50
0
ATc
+
+
-
+
-
+
TATi ΔKu80
TgIscU-HA
cKD TgIscU-HA
cKD TgIscU-HA comp
E
cKD TgSufS-HA
cKD TgIscU-HA
cKD TgSufS-HA
cKD TgIscU-HA
lysis plaques
25
20
15
10
5
0
*
area (mm²)
0.25
0.20
0.15
0.10
0.05
0.00
**

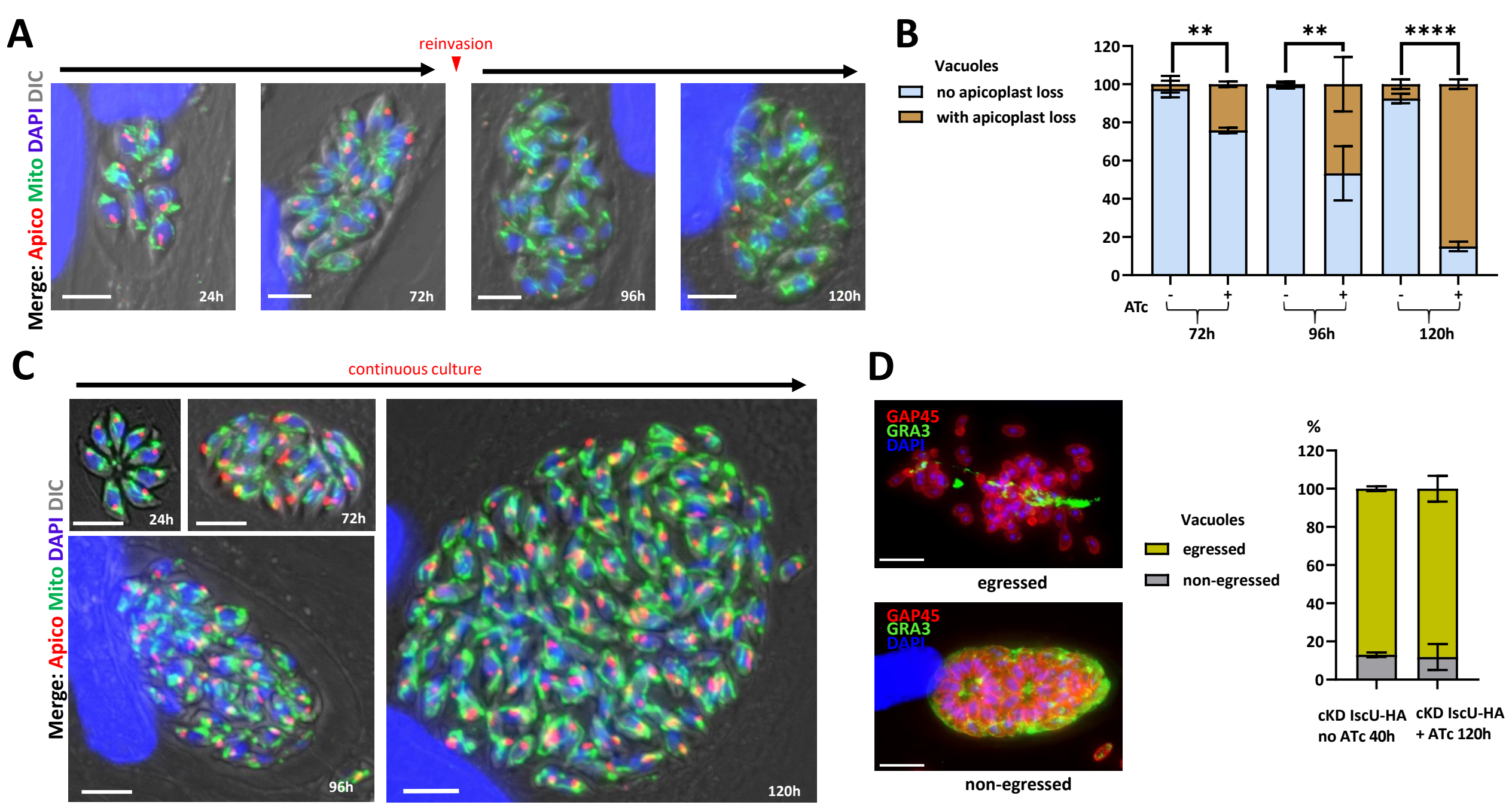
A
reinvasion
Merge: Apico Mito DAPI DIC
24h
72h
96h
120h
B
Vacuoles
no apicoplast loss
with apicoplast loss
**
**
****
120
100
80
60
40
20
0
ATc
-
+
72h
96h
120h
C
continuous culture
Merge: Apico Mito DAPI DIC
24h
72h
96h
120h
D
GAP45
GRA3
DAPI
egressed
non-egressed
Vacuoles
egressed
non-egressed
%
120
100
80
60
40
20
0
cKD IscU-HA no ATc 40h
cKD IscU-HA + ATc 120h

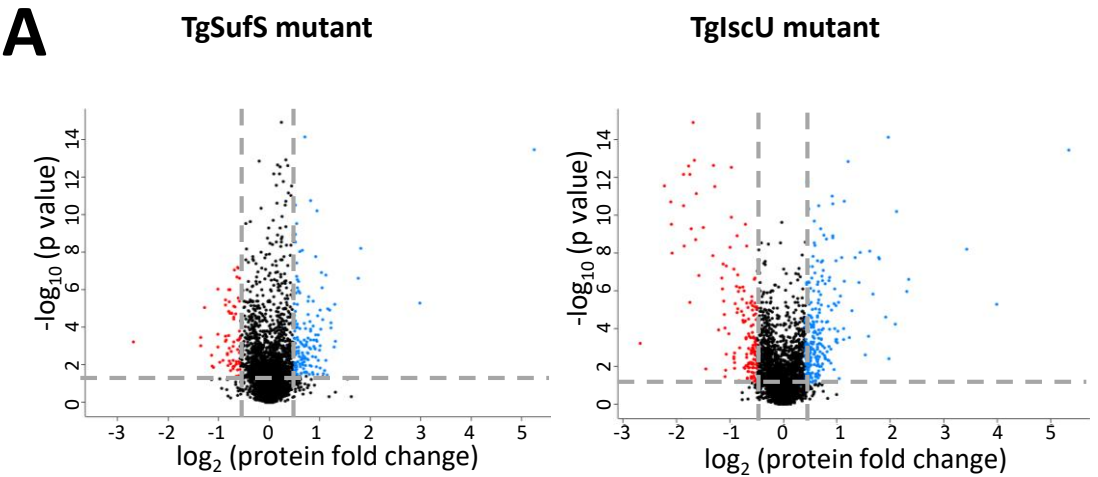
A
TgSufS mutant
TgIscU mutant
-log10 (p value)
log2 (protein fold change)
0
2
4
6
8
10
12
14
-3
-2
-1
0
1
2
3
4
5

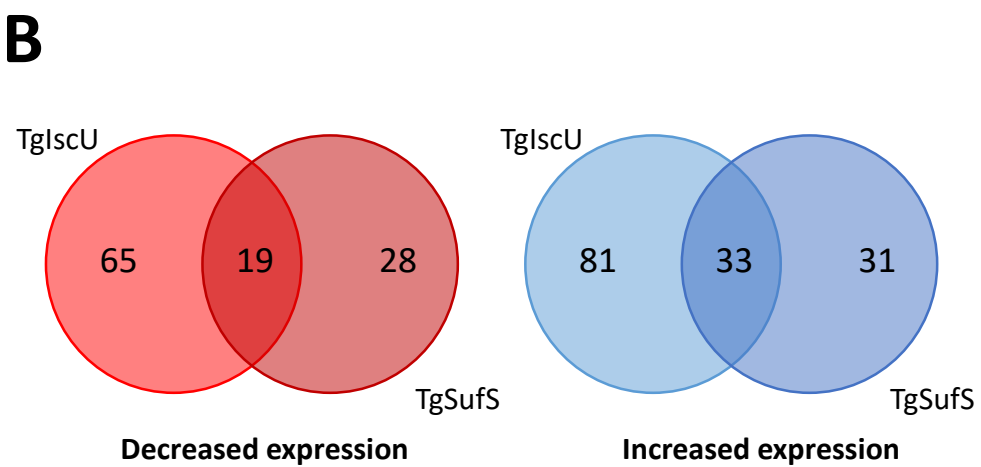
B
TgIscU
65
19
28
TgSufS
Decreased expression
TgIscU
81
33
31
TgSufS
Increased expression

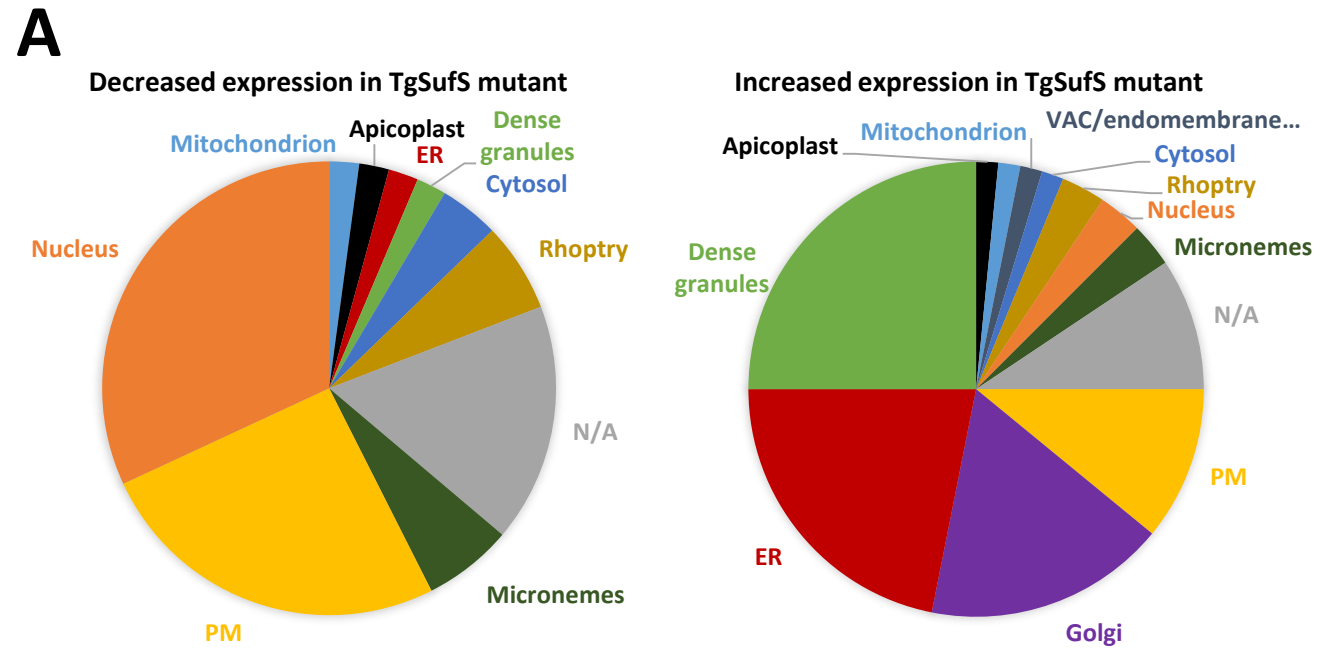
A
Decreased expression in TgSufS mutant
Mitochondrion
Apicoplast
ER
Dense granules
Cytosol
Rhoptry
Nucleus
N/A
Micronemes
PM
Increased expression in TgSufS mutant
Apicoplast
Mitochondrion
VAC/endomembrane...
Cytosol
Rhoptry
Nucleus
Micronemes
N/A
Dense granules
PM
ER
Golgi

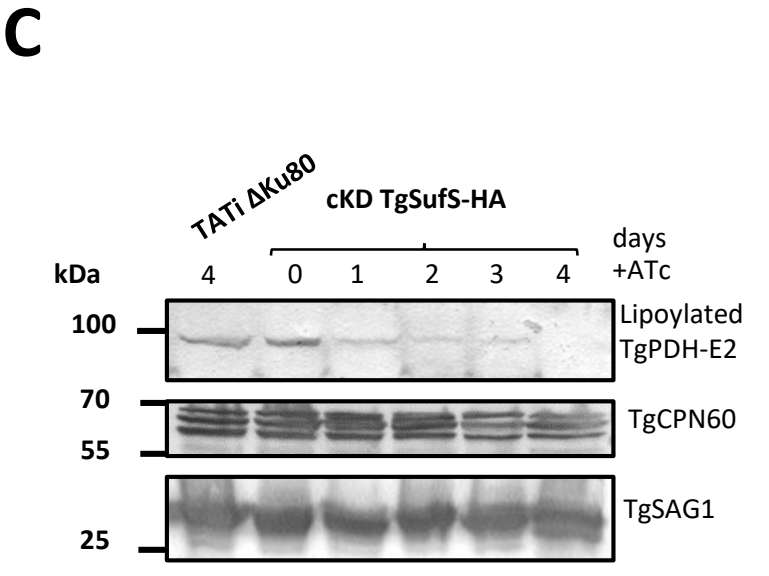
C
TATi ΔKu80
cKD TgSufS-HA
days +ATc
kDa
4
0
1
2
3
4
100
70
55
25
Lipoylated TgPDH-E2
TgCPN60
TgSAG1

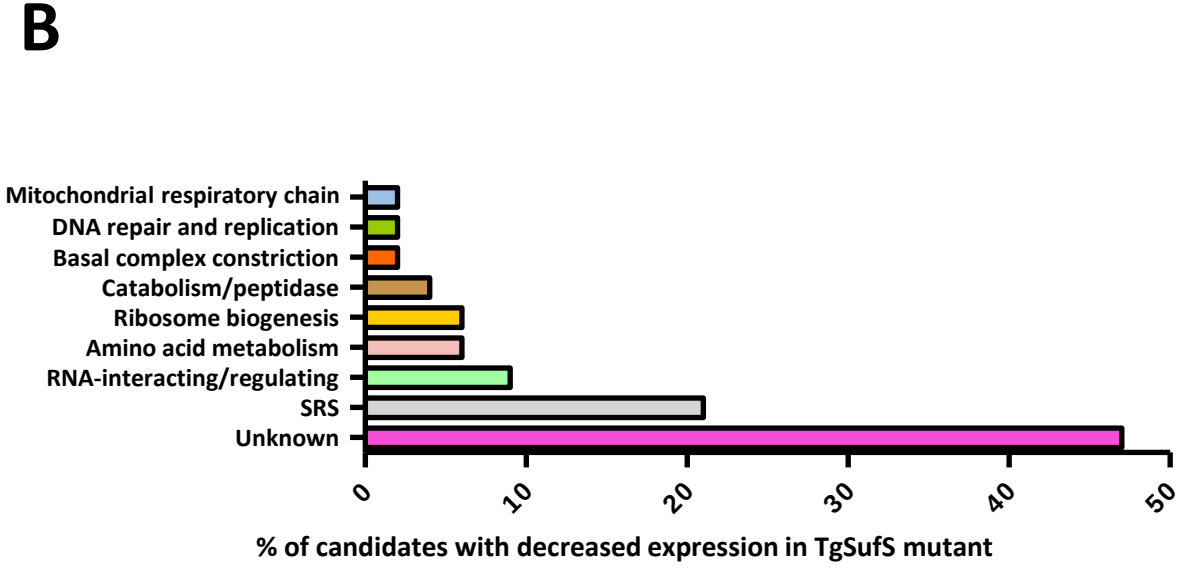
B
Mitochondrial respiratory chain
DNA repair and replication
Basal complex constriction
Catabolism/peptidase
Ribosome biogenesis
Amino acid metabolism
RNA-interacting/regulating
SRS
Unknown
0
10
20
30
40
50
% of candidates with decreased expression in TgSufS mutant

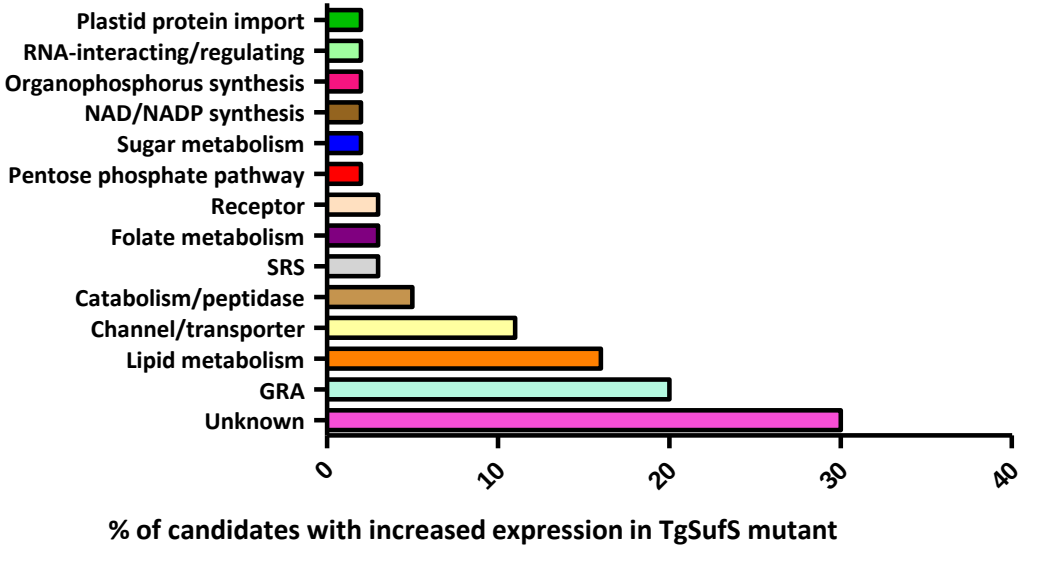
Plastid protein import
RNA-interacting/regulating
Organophosphorus synthesis
NAD/NADP synthesis
Sugar metabolism
Pentose phosphate pathway
Receptor
Folate metabolism
SRS
Catabolism/peptidase
Channel/transporter
Lipid metabolism
GRA
Unknown
0
10
20
30
40
% of candidates with increased expression in TgSufS mutant

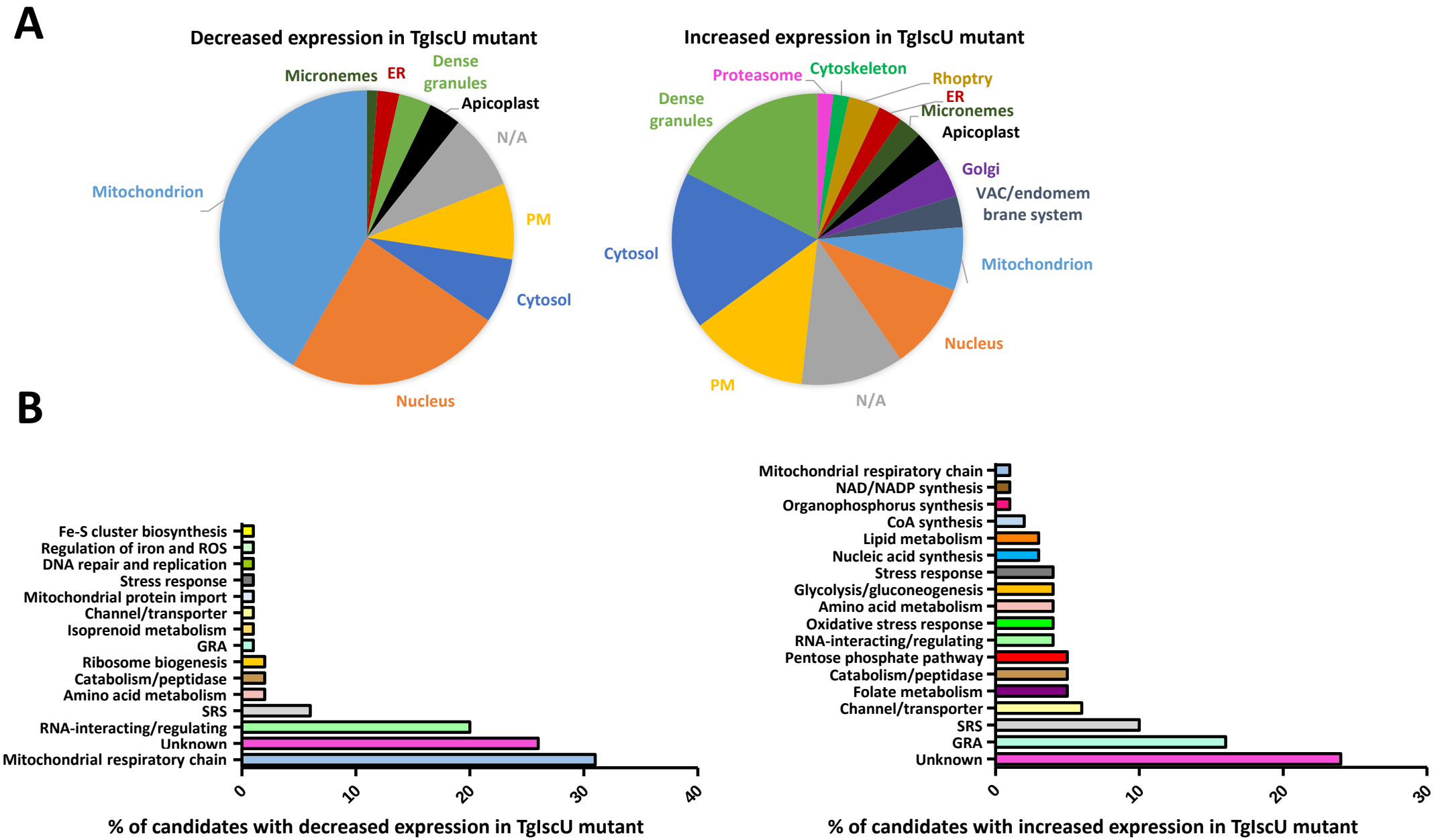
A
Decreased expression in TgIscU mutant
Micronemes
ER
Dense granules
Apicoplast
N/A
PM
Cytosol
Nucleus
Mitochondrion
Increased expression in TgIscU mutant
Proteasome
Cytoskeleton
Rhoptry
ER
Micronemes
Apicoplast
Golgi
VAC/endomembrane system
Mitochondrion
Nucleus
N/A
PM
Cytosol
Dense granules
B
Fe-S cluster biosynthesis
Regulation of iron and ROS
DNA repair and replication
Stress response
Mitochondrial protein import
Channel/transporter
Isoprenoid metabolism
GRA
Ribosome biogenesis
Catabolism/peptidase
Amino acid metabolism
SRS
RNA-interacting/regulating
Unknown
Mitochondrial respiratory chain
0
10
20
30
40
% of candidates with decreased expression in TgIscU mutant
Mitochondrial respiratory chain
NAD/NADP synthesis
Organophosphorus synthesis
CoA synthesis
Lipid metabolism
Nucleic acid synthesis
Stress response
Glycolysis/gluconeogenesis
Amino acid metabolism
Oxidative stress response
RNA-interacting/regulating
Pentose phosphate pathway
Catabolism/peptidase
Folate metabolism
Channel/transporter
SRS
GRA
Unknown
0
10
20
30
% of candidates with increased expression in TgIscU mutant

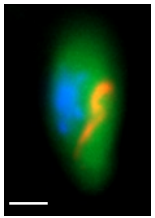

TATi ΔKu80
96h ATc

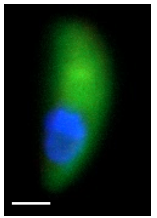

cKD TgIscU-HA
96h ATc

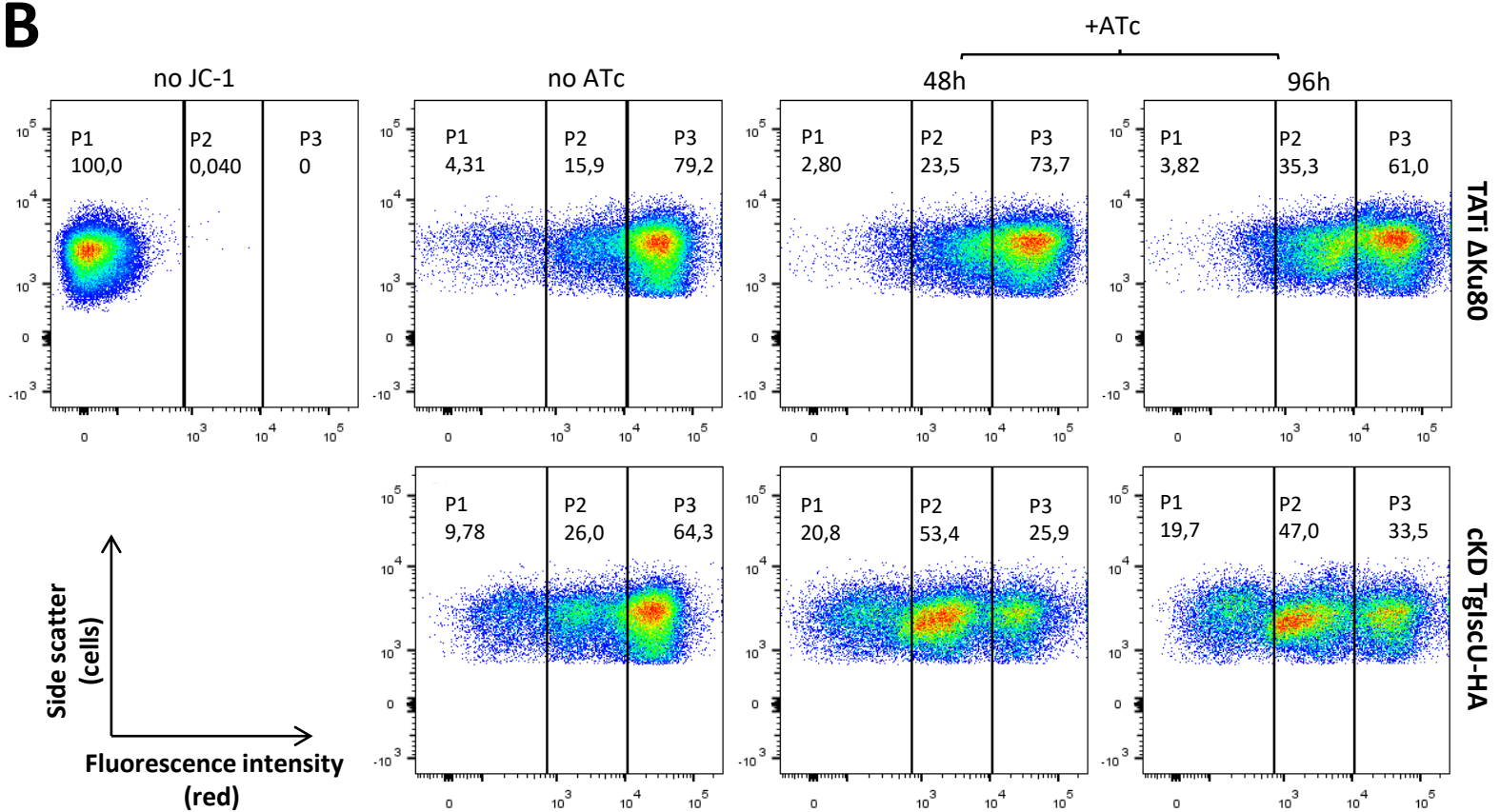

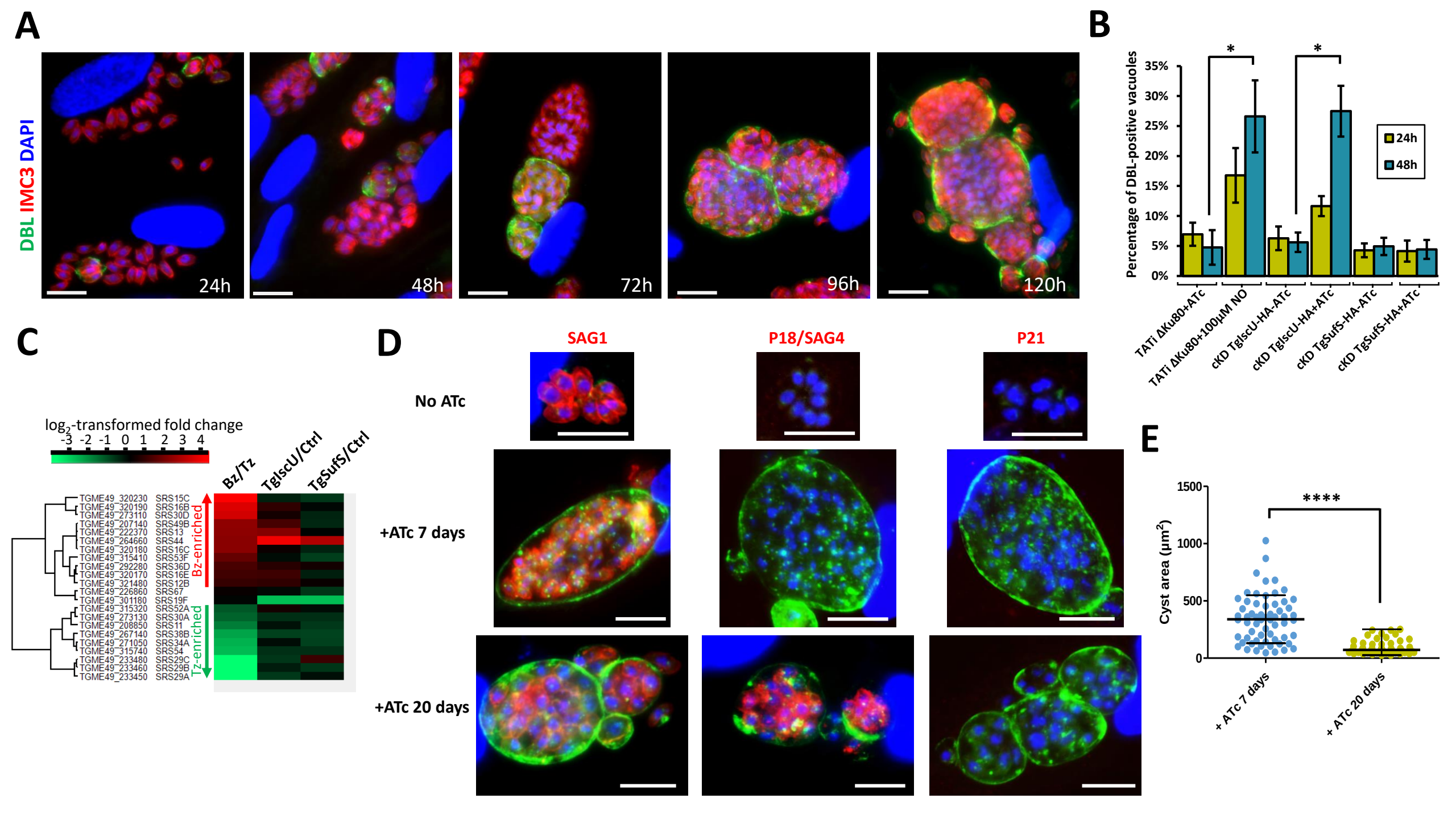
A
DBL IMC3 DAPI
24h
48h
72h
96h
120h
B
Percentage of DBL-positive vacuoles
35%
30%
25%
20%
15%
10%
5%
0%
*
*
24h
48h
TATi ΔKu80+ATc
TATi ΔKu80+100µM NO
cKD TgIscU-HA-ATc
cKD TgIscU-HA+ATc
cKD TgSufS-HA-ATc
cKD TgSufS-HA+ATc
C
log2-transformed fold change
-3 -2 -1 0 1 2 3 4
Bz/Tz
TgIscU/Ctrl
TgSufS/Ctrl
TGME49_320230 SRS15C
TGME49_320190 SRS16B
TGME49_273110 SRS30D
TGME49_207140 SRS49B
TGME49_222370 SRS13
TGME49_264660 SRS44
TGME49_320180 SRS16C
TGME49_315410 SRS53F
TGME49_292280 SRS36D
TGME49_320170 SRS16E
TGME49_321480 SRS12B
TGME49_226860 SRS67
TGME49_301180 SRS19F
TGME49_315320 SRS52A
TGME49_273130 SRS30A
TGME49_208850 SRS11
TGME49_267140 SRS38B
TGME49_271050 SRS34A
TGME49_315740 SRS54
TGME49_233480 SRS29C
TGME49_233460 SRS29B
TGME49_233450 SRS29A
Bz-enriched
Tz-enriched
D
SAG1
P18/SAG4
P21
No ATc
+ATc 7 days
+ATc 20 days
E
Cyst area (µm2)
1500
1000
500
0
****
+ ATc 7 days
+ ATc 20 days